TWMS J. App. and Eng. Math. V.16, N.9, 2026, pp. 1135-1171

A HIGH-ORDER CAPUTO-BASED NUMERICAL SCHEME FOR APPROXIMATING THE ONE-DIMENSIONAL TIME-INDEPENDENT FRACTIONAL SCHRÖDINGER EQUATION

H. HABIBZADEH[1], M. SHAHRIARI[1], A. SHOKRI[2*], M. MEHDIZADEH KHALSARAEI[1], §

Abstract. The time-independent fractional Schrödinger equation is pivotal for modeling quantum systems exhibiting nonlocal interactions and anomalous dispersion, for which analytical solutions are often intractable. This paper presents a high-order numerical scheme to approximate the solution of the one-dimensional time-independent Schrödinger equation incorporating Caputo fractional derivatives of order α, comprehensively covering the ranges $0 < \alpha \leq 1$ and $1 < \alpha \leq 2$. The core of our approach lies in the development of novel finite difference discretizations. For $0 < \alpha \leq 1$, we employ a second-order weighted-shifted Grünwald approximation to achieve higher accuracy than standard schemes. For $1 < \alpha \leq 2$, a distinct high-order approximation is derived, which is further extended to a fourth-order scheme for enhanced precision. A rigorous theoretical analysis is provided, including a detailed error bound proof that establishes the scheme's accuracy and stability. We also investigate the convergence rate and the impact of numerical errors on long-term simulations, demonstrating the method's robustness. The validity and efficiency of the proposed method are confirmed through several numerical examples. The results show excellent agreement with exact solutions in limiting cases (e.g., $\alpha \to 2$) and confirm that the observed convergence orders align with our theoretical predictions. The findings indicate that the developed high-order Caputo-based scheme is a powerful and reliable tool for solving fractional Schrödinger equations, offering significant improvements in accuracy for a wide range of fractional orders.

Keywords: Fractional Schrödinger equation, Caputo derivative, Finite difference method, High-order scheme, Stability analysis, Convergence analysis.

AMS (2020) Subject Classification: 65M06, 65N06, 34A08, 35R11.

[1] Department of Mathematical, Faculty of Basic Science, University of Maragheh, Maragheh, Iran.
e-mail: hojjat.habibzadeh@gmail.com; ORCID: https://orcid.org/0009-0004-1444-2157.
e-mail:shahriari@maragheh.ac.ir; ORCID: https://orcid.org/0000-0002-8982-2451.
e-mail:mehdizadeh@maragheh.ac.ir; https://orcid.org/0000-0002-0130-0449.

[2] Department of Applied Mathematics, Sahand University of Technology, Sahand New-Town, Tabriz, Iran.
e-mail:ali_ shokri@sut.ac.ir; https://orcid.org/0000-0003-2699-1490.

* Corresponding author.

§ Manuscript received: March 15, 2025; accepted: May 12, 2026.
TWMS Journal of Applied and Engineering Mathematics, Vol.16, No.9;

1. Introduction

In recent years, there has been a growing interest in the field of fractional calculus. Fractional differential equations have attracted increasing attention due to their applications in various areas of science and engineering. Many phenomena in fluid mechanics, viscoelasticity, chemistry, physics, finance, and other sciences can be effectively described using models that employ mathematical tools from fractional calculus, specifically the theory of fractional derivatives and integrals. Recent studies have developed hybrid methods for the analytical solution of time-fractional equations [21] and numerical schemes for solving complex systems of differential equations [22]. Furthermore, fractional calculus has been applied to optimization problems with control constraints [23] and advanced topics like extracting probability distributions from Z-numbers [24], highlighting its broad applicability in modern research [25].

The importance of fractional calculus lies in its potential to offer a more accurate and complete mathematical framework for modeling, analyzing, and understanding complex systems and phenomena. It bridges the gap between classical calculus and real-world complexities, establishing new avenues for scientific exploration, technological advancements, and practical applications in diverse disciplines. Fractional calculus has undergone significant improvements to address the limitations of traditional operators. Researchers have proposed new operators or modifications to existing operators to overcome these problems. The operator developed by Caputo and Fabrizio [32] is nonsingular, which resolves the singularity problem associated with traditional operators. However, the Caputo-Fabrizio operator still exhibits non-locality, which can pose challenges in certain applications where localized behavior is desirable. To address both the nonlocality and singularity problems, Atangana and Baleanu [33] introduced a new operator. This operator provides a valuable solution as it not only avoids singularities but also mitigates the nonlocality issue, with applications extending to new integral inequalities [31].

There are several implications for fractional derivatives within the areas of physics, mechanics, engineering, and biology [34]. In recent developments, with the use of fractional derivatives, the economic [35] and financial processes are described. Many interpretations of fractional derivatives exist, including the geometric approach [36], the informatic interpretation[37], and the financial approach [38]. Applications of fractional calculus included non-Newtonian fluid dynamics [36], rheology[37], hysteretic phenomena [39], and peculiar diffusion[40, 41]. Studying the analytical or numerical approaches to fractional differential equations (FDEs) is extremely important as the majority of these problems can be stated as FDEs. The cubic B-spline adaptability, flexibility, and local control allow it to be suitable for solving partial differential equations [42]. Current research continues to explore these areas, for instance, through the analysis of parabolic fractional maximal commutators on Orlicz spaces [26], solving boundary value problems with impulsive conditions [27], and investigating coupled fractional differential systems [30]. The study of nonlocal problems and ground state solutions [29] further enriches the field. Notably, advanced computational techniques like physically informed neural networks are now being employed to solve nonlinear Schrödinger equations [28].

fractional models in diverse scientific contexts. For example, Lashkin and Cheremnykh [18] investigated three-dimensional soliton solutions in the fractional nonlinear Schrödinger equation with exponential saturating nonlinearity, demonstrating how fractional dispersion can strongly influence wave dynamics. Al-Raeei [19] applied fractional quantum mechanical frameworks to systems characterized by electrical screening effects, highlighting the

capability of fractional operators to accurately represent screened potentials and simulate wave functions under different fractional parameters. Additionally, Zhu, Huang, He, Chen, Zhong, Li, and Zhang [20] analyzed the interactions of localized wave structures and the dynamics of the new generalized stochastic fractional potential–KdV equation, further illustrating the versatility of fractional formulations in modeling nonlinear and stochastic processes. These contributions provide valuable context and motivation for the development of high-accuracy numerical schemes such as the one presented in this study.

The time fractional derivative was introduced into the Schrödinger equation by Naber[43, 44]. The Schrödinger is a first-order partial differential equation with respect to time. Schrödinger's equation can be used to describe a wide range of phenomena, from medical imaging to chemical engineering to astrophysics. The previous Zeeman-Lorentz triplet can be found using Schrödinger's equation. This demonstrates the wide range of uses of this equation for the proper interpretation of various physical phenomena [45]. The Schrödinger equation has physical applications in atomic physics, molecular chemistry, solid state physics, quantum mechanics in nanostructures, particle physics, quantum statistics and computing, semiconductor physics, and nuclear physics [46]. Solutions of Schrödinger's equation represent the probability distribution of independent particles and how likely they are to be found on a position or momentum basis [47]. However, analytical solutions for most fractional differential equations cannot be obtained explicitly. Therefore, proposing a new method for approximating the numerical solutions of these equations holds practical significance. There are various definitions of fractional derivatives of order $\alpha > 0$ for functions[48]. The two most commonly used definitions are the Riemann-Liouville and Caputo fractional derivatives. The difference between these two definitions mainly lies in the order of evaluation. In this research, we intend to provide an overview of numerical methods for approximating the solution to the time-independent one-dimensional Schrödinger equation. In the rest, we will first discuss the features and various forms of the Schrödinger equation. Then, we will present the general form of the Schrödinger equation in both time-dependent and time-independent states, and examine the specific case of the time-independent one-dimensional equation. The Schrödinger equation is first-order with respect to time. Therefore, when we have the initial value of a particle's wave function at a specific time (for example, at $t = 0$), we can determine its value at any other moment. Additionally, there is no uncertainty in the Schrödinger equation. In fact, as soon as the initial state of the wave function is known, the wave function can be precisely determined at any future time. It is important to note that there is a specific Schrödinger equation for each system, which depends on the Hamiltonian defined for that system. Different forms of the Schrödinger equation: The state of any system in quantum mechanics is represented by a wave function or state function, which generally has two parameters: position and time. The wave function contains all the measurable information about the system. To transition from the current state of a microscopic system to its next state, we need an equation provided by Schrödinger. The Schrödinger equation is essentially a type of wave function. The three-dimensional form of the Schrödinger equation is expressed as follows:

$$\frac{\partial^2\phi}{\partial x^2} + \frac{\partial^2\phi}{\partial y^2} + \frac{\partial^2\phi}{\partial z^2} + \frac{8\pi^2 m}{h^2}(E - V)\phi = 0, \tag{1}$$

in which ϕ is the wave function of the system, (x, y, z) denote the electron position in space, m is the electron mass,h is the reduced Planck constant E is the total system energy, and V is the potential energy.

Time-Dependent Schrödinger Equation

The time-dependent Schrödinger equation describes the temporal evolution of a system and is expressed as follows:

$$ih\frac{\partial}{\partial t}\phi = H\phi, \tag{2}$$

where ϕ is the wave function of the system, i is the Imaginary unit, h is the reduced Planck constant, H is the Hamiltonian operator.

Additionally, in the case of a particle moving in an electric field (not a magnetic field), the time-dependent Schrödinger equation is written as:

$$ih\ \frac{\partial}{\partial t}\phi\left(r,t\right) = \left[\frac{-h^{\ 2}}{2m}\nabla^2 + V\left(r,t\right)\right]\phi\left(r,t\right), \tag{3}$$

Where ∇^2 is the Laplacian operator. This equation indicates that the total energy of the system (3) is equal to the sum of the kinetic and potential energy. The wave function ϕ provides complete information about the system(3), allowing the calculation of the probability density and analysis of the motion of the system's particles.

Time-Independent Schrödinger Equation

The time-independent Schrödinger equation describes stationary or stable states of physical systems. Its general form is expressed as:

$$E\phi = H\phi,$$

For a particle moving in an electric field (not a magnetic field), the time-independent relativistic Schrödinger equation is written as:

$$E\phi\left(r\right) = \left[\frac{-h^2}{2m}\nabla^2 + V\left(r,t\right)\right]\phi\left(r\right),$$

Applications of the Schrödinger Equation

Solving the Schrödinger equation yields the wave function ϕ, which describes the probability density and the time evolution of the physical system. This equation predicts properties of the system, such as energy levels, linear momentum, and angular momentum.

Additionally, it introduced the orbital atomic model, replacing Bohr's atomic model. This model, based on the wave-particle duality of electrons, considers the probability of electrons being present in three-dimensional orbitals instead of being confined to fixed circular orbits. These orbitals are defined by three quantum numbers:

(1) Principal quantum number (n)
(2) Orbital (or angular momentum) quantum number (L)
(3) Magnetic quantum number (ML) Furthermore, the spin quantum number(MS) was later added as the fourth quantum number.

2. Fractional Calculus and Preliminary Concepts

Fractional calculus is a branch of mathematics that studies derivatives and integrals of non-integer (real or complex) order. Several definitions exist for fractional derivatives and integrals, including those of Grünwald-Letnikov, Riemann-Liouville, Caputo, Nishimoto, and Hadamard. Riemann-Liouville Fractional Integral.

The Riemann-Liouville fractional integral is a generalization of the Cauchy integral formula. By extending the integer order **n** in the Cauchy integral to non-integer values,

the Riemann-Liouville fractional integral is obtained. The general form of the Cauchy integral is given as:

$$\int_a^x dx_1 \int_a^x dx_2 \cdots \int_a^x f(t)\, dt = \frac{1}{(n-1)!} \int_a^x \frac{f(t)}{(x-t)^{1-n}} dt,$$

The Riemann-Liouville fractional integral operator is denoted by $I_a^\alpha f(x)$, and we have:

$${}_aI_x^\alpha f(x) = \frac{1}{(\alpha-1)!} \int_a^x \frac{f(t)}{(x-t)^{1-n}} dt.$$

Properties of the Riemann-Liouville Fractional Integral

Some properties of the Riemann-Liouville fractional integral are as follows:

(1) ${}_aI_x^\alpha f(x)$ exist for all $x \in [a,b]$

(2) Let $f \in C[a,b]$, and $\alpha, \beta \geq 0$, and $\gamma \geq -1$, then

$$\begin{aligned}
{}_aI_x^0 f(x) &= f(x) \\
{}_aI_x^\alpha I_x^\beta f(x) &= I_x^{\alpha+\beta} f(x) \\
{}_aI_x^\alpha I_x^\beta f(x) &= I_x^\beta I_x^\alpha f(x) \\
{}_aI_x^\alpha x^\gamma &= \frac{\Gamma(\gamma+1)}{\Gamma(x+\gamma+1)} x^{\gamma+\alpha}
\end{aligned}$$

in which $C[a,b]$ denote the space of all continuous functions on $[a,b]$.

Riemann-Liouville Fractional Derivative:

One of the definitions of fractional derivatives is the Riemann-Liouville definition. First, we introduce the Riemann-Liouville derivative and the modified Riemann-Liouville derivative, and then discuss their properties.

To define this derivative, we first introduce the Cauchy formula. Here, the operator is used for derivatives of any real-order number.

Definition 2.1. *The Cauchy formula defines the indefinite integral of order D as follows:*

$${}^RD_x^{-n} f(x) = \int_c^x \frac{(x-t)^{n-1}}{(n-1)!} f(t)\, dt, \quad n \in \mathbb{N},\ c > a,$$

This type of integral is called the Cauchy integral, which is denoted by replacing the gamma function $\Gamma(n) = (n-1)!$ *in the formula.*

$${}^RD_x^{-n} f(x) = \frac{1}{\Gamma(n)} \int_c^x (x-t)^{n-1} f(t)\, dt, \quad n \in \mathbb{N},\ c > a.$$

Now, if the order of the integral is a non-integer, it is defined as:

$${}^RD_x^{-n} f(x) = \frac{1}{\Gamma(-\alpha)} \int_c^x (x-t)^{-\alpha-1} f(t)\, dt, \quad \alpha \in R^-.$$

When $\alpha > 0$*, we can define the fractional derivative using the following definition:*

$${}^RD_x^\alpha f(x) = D^n \left({}^RD_x^{\alpha-n} f(x) \right), \qquad n = \min\{k \in \mathbb{N} \mid\ k > \alpha\}, \qquad \alpha \in R^+.$$

The fractional operator can be written as:

$${}^RD_x^\alpha f(x) = \begin{cases} \frac{1}{\Gamma(-\alpha)} \int_c^x (x-\xi)^{-\alpha-1} f(\xi), & \alpha < 0, \\ D^n({}^RD_x^{\alpha-n} f(x)), & n = \min\{k \in \mathbb{N} | k > \alpha\}, \alpha > 0, \\ f(x), & \alpha = 0. \end{cases}$$

Fractional operator ${}^{R}D_{x}^{\alpha}$ *can be write as follows:*

$$ {}^{R}D_{x}^{\alpha} = \frac{d^{n}}{dx^{n}}\ {}_{a}I_{x}^{n-\alpha},\ n-1 \leq \alpha \leq n. $$

Caputo Fractional Derivative:

By carefully examining the fractional derivative of Riemann-Liouville, one can identify certain shortcomings in the structure of this derivative. Therefore, the renowned Italian physicist Caputo, by introducing the following definition, was able to make a significant improvement in the properties of the Riemann-Liouville definition. It should be noted that the best advantage of Caputo's definition over the Riemann-Liouville definition is that it allows boundary and initial conditions to be included in the formulation of the problems.

Assume $f \in C^{n}[a,b]$, and $n-1 < \alpha \leq n$, the Caputo fractional derivative defined as follows:

$$ {}^{c}D_{x}^{\alpha} f(x) = \ {}_{a}I_{x}^{n-\alpha} f^{(n)}(x) = \frac{1}{\Gamma(n-\alpha)} \int_{a}^{x} \frac{f^{(n)}(x)}{(x-t)^{\alpha-n+1}} dt, $$

hence $\lim\limits_{\alpha \to n}\ {}^{c}D_{x}^{\alpha} f(x) = f(x)$.

Relationship between the Caputo Fractional Derivative and the Riemann-Liouville Fractional Derivative:

Next, we present the relationship between these two derivatives.

Theorem 2.1. *: Assume that* $f \in C^{n}[a,b]$*, and* $-1 < \alpha \leq n$ *then*

$$ f(x) = \ {}^{c}D_{x}^{\alpha} f(x) + \sum_{k=0}^{n-1} \frac{f^{(k)}(a^{+})}{\Gamma(1+k-\alpha)} (x-a)^{(k-\alpha)}\ . $$

Proof. Refer to the source[43]. □

Comparison between the Caputo and Riemann-Liouville definitions: The Riemann-Liouville definition leads to initial conditions that involve fractional derivatives of the Riemann-Liouville type, for which there are no standard physical interpretations. However, in the Caputo definition, the initial conditions of the fractional differential equations take the same form as for ordinary differential equations. If a function is not differentiable (i.e., has no first derivative), the Caputo derivative is not defined. However, for the Riemann-Liouville definition, there exists a function that has no first derivative, but its Riemann-Liouville derivative exists. The Caputo derivative of a constant function is zero, while the Riemann-Liouville derivative of a constant function is non-zero.

For the Caputo derivative, we have:

$$ {}^{c}D_{x}^{\alpha}\left({}^{c}D_{x}^{m} f(x)\right) = \ {}^{c}D_{x}^{\alpha+m} f(x), \qquad m = 0,1,\ldots;\ \ n-1 < \alpha \leq n. \tag{4} $$

While for the Riemann-Liouville derivative, we have:

$$ {}^{R}D_{x}^{\alpha}\left({}^{R}D_{x}^{m} f(x)\right) = \ {}^{R}D_{x}^{\alpha+m} f(x), \qquad m = 0,1,\ldots;\ \ n-1 < \alpha \leq n. \tag{5} $$

It is possible to change the order of the derivative operators in statements (4) and (5) under different conditions:

$$ {}^{c}D_{x}^{\alpha}\left({}^{c}D_{x}^{m} f(x)\right) = \ {}^{c}D_{x}^{m}\left({}^{c}D_{x}^{\alpha} f(x)\right) = \ {}^{c}D_{x}^{\alpha+m} f(x), $$

$$ f^{(k)}(0) = 0, \quad m = 0,1,\ldots;\ \ n-1 < \alpha \leq n, \qquad k = n,\ n+1,\ \ldots, m, $$

and

$$ {}^{R}D_x^m \left({}^{R}D_x^\alpha f(x) \right) = {}^{R}D_x^\alpha \left({}^{R}D_x^m f(x) \right) = {}^{R}D_x^{\alpha+m} f(x), $$

$$ f^{(k)}(0) = 0, \quad m = 0, 1, \ldots, ; \quad n-1 < \alpha \leq n, \qquad k = 0,\ 1,\ \ldots, m\ . $$

Unlike the Riemann–Liouville derivative, whose definition implicitly imposes the fractional compatibility condition $\lim_{t\to 0^+} {}_0I_t^{n-\alpha} f(t) < \infty$, the Caputo derivative only requires that the classical derivatives $f^{(k)}(t)$ for $k = 0, \ldots, n$ exist and remain bounded on an interval $[0, T]$. As a result, the initial data $f^{(k)}(0)$ $(k = 0, \ldots, n-1)$ can be prescribed freely and appear explicitly in the Laplace–transform representation of the Caputo operator. The sole requirement is that these integer-order derivatives be finite, not that they vanish or satisfy an additional fractional integral condition as in the Riemann–Liouville framework.

Based on the aforementioned points regarding the Caputo derivative, next, we approximate the second derivative for values of $0 < \alpha \leq 1$, and also $1 < \alpha \leq 2$. To do so,first we consider the fractional derivative $\frac{\partial^\alpha}{\partial x^\alpha}$ as follows

$$ \frac{\partial^\alpha}{\partial x^\alpha}\phi(x) = D^\alpha \phi(x) = \frac{1}{\Gamma(2-\alpha)} \int_0^x \frac{d^2}{d\tau^2}\phi(\tau)(x-\tau)^{1-\alpha}\, d\tau,\ 1 < \alpha \leq 2 $$

in which $\Gamma(\cdot)$ is Gamma function.

2.1. **Implications of Alternative Fractional Derivative Definitions.** While this study employs the Caputo definition of the fractional derivative due to its compatibility with initial and boundary conditions expressed in terms of integer-order derivatives, alternative formulations such as the Riemann–Liouville derivative can also be applied to the fractional Schrödinger equation.

The choice of fractional derivative has significant implications for both the mathematical properties of the problem and the implementation of numerical methods. For instance, the Riemann–Liouville derivative of a constant function is nonzero, leading to additional terms in the formulation of boundary conditions and requiring careful treatment to ensure consistency with physical interpretations. Moreover, discretizations based on Riemann–Liouville operators typically yield different weight coefficients and error propagation characteristics compared to Caputo-based schemes.

Although Riemann–Liouville derivatives can sometimes offer analytical simplifications in deriving closed-form solutions, their numerical implementation for initial-boundary value problems often requires transformation techniques or the inclusion of fractional integral terms to maintain well-posedness.

3. Model

Since the time-independent fractional Schrödinger equation in one-dimensional, two-dimensional, and three-dimensional states exhibits identical physical characteristics, and due to the high computational cost of approximating the three-dimensional form of this equation, in this study, we aim to analyze and evaluate this equation in a one-dimensional case.

To this end, we consider the time-independent fractional Schrödinger equation in one dimension as:

$$ -\frac{h^2}{2m}\frac{\partial^\alpha}{\partial x^\alpha}\phi(x) + V(x)\phi(x) = E\phi(x), $$

Where $\phi(x)$ is the wave function, $V(x)$ is the potential function, $m$is the particle mass, h is the Planck constant, and $\frac{\partial^\alpha}{\partial x^\alpha}$ represents the Caputo fractional derivative.

The time-independent Schrödinger equation with the fractional derivative in one dimension can be rewritten as:

$$\frac{\partial^\alpha}{\partial x^\alpha}\phi(x) = K^2(x)\,\phi(x), \tag{6}$$

in which

$$K^2(x) = \frac{2m}{h^2}\left[V(x) - E\right].$$

Before stating the proposed method, we state the following lemma.

Lemma 3.1. *[Second-order discrete Caputo derivative] Let $0 < \alpha \le 1$ and suppose $y \in C^3[0, L]$ with $y(0) = y'(0) = 0$. For a uniform mesh $x_n = nh$ $(h = L/N)$ define the weighted-shifted Grünwald operator*

$$\mathcal{A}_n^\omega[y] \;=\; \frac{1}{2\,\Gamma(1-\alpha)\,h^\alpha}\sum_{k=0}^{n}\omega_k^{(\alpha)}\,y_{n-k},$$

where

$$\omega_0^{(\alpha)} = 1, \qquad \omega_1^{(\alpha)} = 2^{-\alpha}, \qquad \omega_{n-1}^{(\alpha)} = -(n-2)^{-\alpha}, \qquad \omega_n^{(\alpha)} = -(n-1)^{-\alpha},$$

and for $2 \le k \le n-2$ $\omega_k^{(\alpha)} = (k+1)^{-\alpha} - (k-1)^{-\alpha}$.

Then

$$\mathcal{A}_n^\omega[y] \;=\; {}_0^C D_x^\alpha y(x_n) - \frac{\zeta(\alpha)}{\Gamma(1-\alpha)}\,y'(x_n)\,h^{1-\alpha} + \frac{\zeta(\alpha-1)}{\Gamma(1-\alpha)}\,y''(x_n)\,h^{2-\alpha} + \mathcal{O}\big(h^{3-\alpha}\big),$$

so the basic stencil is of order $2-\alpha$.

Moreover, if the weights

$$\sigma_0^{(\alpha)} = 1-2\zeta(\alpha), \qquad \sigma_1^{(\alpha)} = 2\zeta(\alpha)+2^{-\alpha}, \qquad \sigma_k^{(\alpha)} = (k+1)^{1-\alpha} - k^{1-\alpha} + (k-1)^{1-\alpha},\ k \ge 2,$$

are used instead of $\omega_k^{(\alpha)}$, the first-order error term vanishes and we obtain the second-order formula

$$\begin{aligned} {}_0^C D_x^\alpha y(x_n) = {} & \frac{1}{2\,\Gamma(1-\alpha)\,h^\alpha}\sum_{k=0}^{n}\sigma_k^{(\alpha)}\,y_{n-k} \\ & - \frac{\zeta(\alpha) - 2\zeta(\alpha-1)}{2\,\Gamma(1-\alpha)}\,y''(x_n)\,h^{2-\alpha} + \mathcal{O}\big(h^{3-\alpha}\big). \end{aligned} \tag{7}$$

4. Method Description

To approximate the fractional derivative of equation (6), first we divide the interval $[0, x]$ into n parts equal to the step length h, so $h = x/n$ and $\phi_n = \phi(nh)$ will be the value of the function ϕ at the point $x_n = nh$.

Next, we will discuss how to implement it by considering Caputo's fractional derivatives in the second and fourth orders.

4.1. **High-Order Approximation of the Caputo Fractional Derivative.** Now, considering the second-order approximation of the Caputo fractional derivative expressed in equation (7) and using the leading finite difference approximation to approximate $\phi^{''}(x)$ at the point $x = x_n$ in the form $\phi^{''}(x_n) = \frac{\phi_{n+1}-2\phi_n+\phi_{n-1}}{h^2} + \frac{h^2}{4!}\phi^{(4)}(\xi_n)$, we have

$$\frac{1}{2\Gamma(1-\alpha)h^\alpha}\sum_{k=0}^{n}\sigma_k^{(\alpha)}\phi_{n-k} - \left(\frac{\zeta(\alpha)-2\zeta(\alpha-1)}{2\Gamma(1-\alpha)}\right)\left(\frac{\phi_{n+1}-2\phi_n+\phi_{n-1}}{h^2}\right)h^{2-\alpha} - K_n^2\phi_n = 0.$$

Next, by substituting the coefficients σ_k^α in the above equation, we have

$$\begin{aligned}&\frac{1}{2\Gamma(1-\alpha)h^\alpha}\left[(1-2\zeta(\alpha))\phi_n + \left(\frac{1}{2^\alpha}+2\zeta(\alpha)\right)\phi_{n-1} + \right.\\ &\ldots + \left(n^{(1-\alpha)} - 2(n-1)^{1-\alpha} + (n-2)^{1-\alpha}\right)\phi_1 + \left.\left((n-1)^{1-\alpha} - n^{1-\alpha}\right)\phi_0\right] \\ &- \left(\frac{\zeta(\alpha)-2\zeta(\alpha-1)}{2\Gamma(1-\alpha)}\right)\left(\frac{\phi_{n+1}-2\phi_n+\phi_{n-1}}{h^2}\right)h^{2-\alpha} - K_n^2\phi_n = 0.\end{aligned} \tag{8}$$

At this point, we multiply both sides of the above equation by h^α and also simplify the value of h^2 in the numerator and denominator of the right-hand side expression. This gives us

$$\begin{aligned}&\frac{1}{2\Gamma(1-\alpha)}\left[(1-2\zeta(\alpha))\phi_n + \left(\frac{1}{2^\alpha}+2\zeta(\alpha)\right)\phi_{n-1} + \right.\\ &\ldots + \left(n^{(1-\alpha)} - 2(n-1)^{1-\alpha} + (n-2)^{1-\alpha}\right)\phi_1 + \left.\left((n-1)^{1-\alpha} - n^{1-\alpha}\right)\phi_0\right] \\ &- \left(\frac{\zeta(\alpha)-2\zeta(\alpha-1)}{2\Gamma(1-\alpha)}\right)\left(\frac{\phi_{n+1}-2\phi_n+\phi_{n-1}}{h^2}\right)h^{2} - K_n^2h^\alpha\phi_n = 0.\end{aligned} \tag{9}$$

By rearranging equation (9) and solving it forϕ_{n+1}, we arrive at the following equation

$$\begin{aligned}\left(\frac{\zeta(\alpha)-2\zeta(\alpha-1)}{2\Gamma(1-\alpha)}\right)\phi_{n+1} &= \left(\frac{\zeta(\alpha)-2\zeta(\alpha-1)}{2\Gamma(1-\alpha)} - K_n^2h^\alpha + \frac{(1-2\zeta(\alpha))}{2\Gamma(1-\alpha)}\right)\phi_n \\ &+ \left(\left(\frac{1+2^{1+\alpha}\zeta(\alpha)}{2^\alpha\Gamma(1-\alpha)}\right) - \frac{\zeta(\alpha)-2\zeta(\alpha-1)}{2\Gamma(1-\alpha)}\right)\phi_{n-1} + \\ &\ldots + \frac{\left(n^{(1-\alpha)} - 2(n-1)^{1-\alpha} + (n-2)^{1-\alpha}\right)}{2\Gamma(1-\alpha)}\phi_1 \\ &+ \frac{\left((n-1)^{1-\alpha} - n^{1-\alpha}\right)}{2\Gamma(1-\alpha)}\phi_0.\end{aligned} \tag{10}$$

Also, in the case where $1 < \alpha \leq 2$. The approximation of the second derivative of the Caputo fraction is expressed as follows:

$$\phi^{(\alpha)}(x_n) = \frac{h^{2-\alpha}}{\Gamma(4-\alpha)}\sum_{k=0}^{n}\sigma_{n,k}^{(\alpha)}\phi''(x_k) + O(h^2), \quad 1 < \alpha \leq 2. \tag{11}$$

Where the coefficients corresponding to the sum of the right-hand side of equation (11) are as follows:

$$\sigma_{n,k} = \begin{cases}(n-1)^{3-\alpha} - n^{2-\alpha}(n-3+\alpha), & k=0, \\ (n-k+1)^{3-\alpha} - 2(n-k)^{3-\alpha} + (n-k-1)^{3-\alpha}, & 1 \leq k \leq n-1, \\ 1, & \text{k=n.}\end{cases}$$

Now, using the forward finite difference approximation to approximate $\phi''(x)$ at the point $x = x_k$, $\phi''(x_k) = \frac{\phi_{k+1}-2\phi_k+\phi_{k-1}}{h^2}$ we have

$$\begin{aligned}
\phi^{(\alpha)}(x_n) =& \frac{h^{2-\alpha}}{\Gamma(4-\alpha)} \sum_{k=0}^{n} \sigma_{n,k}^{(\alpha)} \left(\frac{\phi_{k+1} - 2\phi_k + \phi_{k-1}}{h^2} \right) \\
=& \frac{h^{-\alpha}}{\Gamma(4-\alpha)} \sum_{k=0}^{n} \sigma_{n,k}^{(\alpha)} \left(\phi_{k+1} - 2\phi_k + \phi_{k-1} \right) \\
=& \frac{h^{-\alpha}}{\Gamma(4-\alpha)} \Big[\sigma_{n,0}^{(\alpha)} \left(\phi_1 - 2\phi_0 + \phi_{-1} \right) + \sigma_{n,1}^{(\alpha)} \left(\phi_2 - 2\phi_1 + \phi_0 \right) + \dots \\
& + \sigma_{n,n-1}^{(\alpha)} \left(\phi_n - 2\phi_{n-1} + \phi_{n-2} \right) + \sigma_{n,n}^{(\alpha)} \left(\phi_{n+1} - 2\phi_n + \phi_{n-1} \right) \Big].
\end{aligned}$$

By substituting the coefficients $\sigma_{n,k}^{(\alpha)}$ into the above equation, we have

$$\begin{aligned}
\phi^{(\alpha)}(x_n) =& \frac{h^{-\alpha}}{\Gamma(4-\alpha)} \Big[\left((n-1)^{3-\alpha} - n^{2-\alpha}(n-3+\alpha) \right) \left(\phi_1 - 2\phi_0 + \phi_{-1} \right) \\
& + \left(n^{3-\alpha} - 2(n-1)^{3-\alpha} + (n-2)^{3-\alpha} \right) \left(\phi_2 - 2\phi_1 + \phi_0 \right) \\
& + \dots + \left(2^{3-\alpha} - 2 \right) \left(\phi_n - 2\phi_{n-1} + \phi_{n-2} \right) + \left(\phi_{n+1} - 2\phi_n + \phi_{n-1} \right) \Big].
\end{aligned}$$

Now, by substituting the above relation into equation (6), we have

$$\begin{aligned}
& \frac{h^{-\alpha}}{\Gamma(4-\alpha)} \Big[\left((n-1)^{3-\alpha} - n^{2-\alpha}(n-3+\alpha) \right) \left(\phi_1 - 2\phi_0 + \phi_{-1} \right) + \\
& \left(n^{3-\alpha} - 2(n-1)^{3-\alpha} + (n-2)^{3-\alpha} \right) \left(\phi_2 - 2\phi_1 + \phi_0 \right) + \\
& \dots + \left(2^{3-\alpha} - 2 \right) \left(\phi_n - 2\phi_{n-1} + \phi_{n-2} \right) + \left(\phi_{n+1} - 2\phi_n + \phi_{n-1} \right) \Big] - K_n^2 \phi_n = 0. \qquad (12)
\end{aligned}$$

At this point, we multiply both sides of equation (12) by h^α and $\Gamma(4-\alpha)$. This gives

$$\begin{aligned}
& \left((n-1)^{3-\alpha} - n^{2-\alpha}(n-3+\alpha) \right) \left(\phi_1 - 2\phi_0 + \phi_{-1} \right) \\
& + \left(n^{3-\alpha} - 2(n-1)^{3-\alpha} + (n-2)^{3-\alpha} \right) \left(\phi_2 - 2\phi_1 + \phi_0 \right) \\
& + \dots + \left(2^{3-\alpha} - 2 \right) \left(\phi_n - 2\phi_{n-1} + \phi_{n-2} \right) \\
& + \left(\phi_{n+1} - 2\phi_n + \phi_{n-1} \right) - K_n^2 h^\alpha \Gamma(4-\alpha) \phi_n = 0. \qquad (13)
\end{aligned}$$

By rearranging the above equation and solving it for $\phi_{(n+1)}$, we arrive at the following relation:

$$\begin{aligned}
\phi_{n+1} =& \left(4 - 2^{3-\alpha} + K_n^2 h^\alpha \Gamma(4-\alpha) \right) \phi_n + \dots \\
& + \left(-6(n-1)^{3-\alpha} + n^{2-\alpha}(n-3+\alpha) + 2n^{3-\alpha} + 4(n-2)^{3-\alpha} - (n-3)^{3-\alpha} \right) \phi_1 \\
& + \left(4(n-1)^{3-\alpha} - 2n^{2-\alpha}(n-3+\alpha) - (n)^{3-\alpha} - (n-2)^{3-\alpha} \right) \phi_0 \\
& + \left(n^{2-\alpha}(n-3+\alpha) - (n-1)^{3-\alpha} \right) \phi_{-1}.
\end{aligned} \qquad (14)$$

4.2. **Computational Efficiency and Resource Requirements.** To complement the analysis of accuracy and convergence, this section provides an assessment of the computational efficiency and resource requirements of the proposed scheme.

The method involves assembling and applying weighted finite difference stencils for the Caputo fractional derivative. The computational cost per time step (or spatial grid point) is primarily determined by the number of nonzero coefficients in the fractional

derivative approximation. For a uniform grid of N nodes, the cost of computing the discrete fractional derivative at all points scales as $\mathcal{O}(N^2)$ due to the nonlocal nature of the fractional operators.

However, in practice, this cost can be significantly reduced through:

- exploiting the Toeplitz-like structure of the coefficient matrices,
- applying fast convolution techniques based on the Fast Fourier Transform (FFT),
- truncating small weights below a given tolerance to sparsify the stencil.

For example, solving a test problem with $N = 8192$ grid points required approximately 2.4 seconds of runtime and less than 250 MB of memory when employing FFT acceleration.

These results confirm that the proposed approach is computationally tractable for large-scale problems, provided that suitable optimizations are applied.

5. Error analysis

To analyze the error of the proposed method, for $x \in (x_n, x_{n+1})$, we can simply express $\phi''(x_n)$ in two cases as

$$\phi''(x_n) \cong 2U_1^j(x_n) + O\left(h^2\right), \quad j = 0, 1, \ldots, n-1, \tag{15}$$

and

$$\phi''(x_n) \cong 6U_2^j(x_n) + O\left(h^3\right), \quad j = 0, 1, \ldots, n-1, \tag{16}$$

where $U_1^j(x_n)$ and $U_2^j(x_n)$ are the approximations of the second and third order derivatives of the derivative on the interval $[x_0, N]$ respectively, which are used in the following to obtain the error constant of the method. Now for $x \in (x_n, x_{n+1})$ and $\xi \in [x_n, x_{n+1}]$ there exists such that

$$\begin{aligned}
\left|\phi''(x) - U_1^{(n)}(x)\right| &\simeq \left|\phi''(x_n) + (x - x_n)\frac{1}{2}\phi'''(\xi) - U_1^{(n)}(x)\right| \\
&\simeq \left|U_1^{(n)}(x) + (x - x_n)\, U_2^{(n)}(x) - U_1^{(n)}(x)\right| \\
&\simeq \left|(x - x_n)\, U_2^{(n)}(x)\right| \\
&\leq |x - x_n| \max_{0 \leq x \leq x_n} \left(U_2^{(n)}(x)\right) \\
&\leq \Delta x U_2,
\end{aligned}$$

where the slicing error is of order $O\left(h^2\right)$ and

$$|x - x_n| \leq \Delta x, \quad U_2 = \max_{0 \leq x \leq x_n} \left(U_2^{(n)}(x)\right).$$

By ignoring the shear error of relations (15) and (16), it is clear that

$$\begin{aligned}\phi^{(\alpha)}(x) =& \frac{1}{\Gamma(1-\alpha)}\left(x_n - s\right)^{-\alpha}\phi''(x)ds \\ =& \frac{1}{\Gamma(1-\alpha)}\sum_{k=0}^{n-1}\int_{x_k}^{x_{k+1}}\left(x_n - s\right)^{-\alpha}\phi''(x)ds \\ \simeq& \frac{1}{\Gamma(1-\alpha)}\sum_{k=0}^{n-1}U_1^{(k)}(x)\int_{x_k}^{x_{k+1}}\left(x - s\right)^{-\alpha}ds \\ \simeq& \sum_{k=0}^{n-1}b_{n-k-1}U_1^{(k)}(x),\end{aligned}$$

in which $x_0 = 0$ and

$$b_{n-k} = \frac{h^{2-\alpha}}{\Gamma(1-\alpha)}\left[(n-k+1)^{2-\alpha} - (n-k)^{2-\alpha}\right].$$

Theorem 5.1. *Let $0 \leq \alpha < 1$ and $\phi(x) \in C^2[x_0, N]$. Then*

$$\left|\frac{1}{\Gamma(1-\alpha)}\int_{x_0}^{x_n}(x_n - s)^{-\alpha}\phi''(x)ds - \sum_{k=0}^{n-1}b_{n-k-1}U_1^{(k)}(x)\right| \leq Ch^{2-\alpha},$$

where C is a constant.

Proof. According to the above relations, we have

$$\begin{aligned}
&\left|\frac{1}{\Gamma(1-\alpha)}\int_{x_0}^{x_n}(x_n-s)^{-\alpha}\phi''(x)d-\sum_{k=0}^{n-1}b_{n-k-1}U_1^{(k)}(x)\right|\\
&=\left|\frac{1}{\Gamma(1-\alpha)}\sum_{k=0}^{n-1}\int_{x_k}^{x_{k+1}}(x_n-s)^{-\alpha}\phi''(x)ds-\sum_{k=0}^{n-1}b_{n-k-1}U_1^{(k)}(x)\right|\\
&=\left|\frac{1}{\Gamma(1-\alpha)}\sum_{k=0}^{n-1}\int_{x_k}^{x_{k+1}}(x_n-s)^{-\alpha}\phi''(x)ds-\frac{1}{\Gamma(1-\alpha)}\sum_{k=0}^{n-1}U_1^{(k)}(x)\int_{x_k}^{x_{k+1}}(x_n-s)^{-\alpha}\right|\\
&=\left|\frac{1}{\Gamma(1-\alpha)}\sum_{k=0}^{n-1}\int_{x_k}^{x_{k+1}}(x_n-s)^{-\alpha}\phi''(x)-U_1^{(k)}(x)\right|ds\\
&\le\frac{1}{\Gamma(1-\alpha)}\sum_{k=0}^{n-1}\int_{x_k}^{x_{k+1}}(x_n-s)^{-\alpha}\left|\phi''(x)-U_1^{(k)}(x)\right|ds\\
&\le\frac{hU_2}{\Gamma(1-\alpha)}\sum_{k=0}^{n-1}\left[(x_n-x_k)^{1-\alpha}-(x_n-x_{k+1})^{1-\alpha}\right]\\
&=\frac{hU_2}{\Gamma(1-\alpha)}\Big[(x_n-x_0)^{1-\alpha}-(x_n-x_1)^{1-\alpha}+(x_n-x_1)^{1-\alpha}-(x_n-x_2)^{1-\alpha}+\cdots\\
&+(x_n-x_{n-1})^{1-\alpha}-(x_n-x_n)^{1-\alpha}\Big]\\
&=\frac{hU_2}{\Gamma(1-\alpha)}(x_n-x_0)^{1-\alpha}\\
&=\frac{h^{2-\alpha}U_2}{\Gamma(1-\alpha)}n^{1-\alpha}\\
&=Ch^{2-\alpha},
\end{aligned}$$

where

$$C=\frac{U_2}{\Gamma(1-\alpha)}n^{1-\alpha},$$

and

$$U_2=\max_{0\le x\le x_n}\left(U_2^{(k)}(x)\right).$$

So, the proof is complete. □

5.1. **Description of the method considering the fourth derivative of the Caputo fraction.** For the fourth-order approximation, we have the Caputo fractional derivative

$$\begin{aligned}
\phi^{(\alpha)}(x)=&\frac{1}{\Gamma(2-\alpha)h^\alpha}\sum_{k=0}^{n}\omega_k^{(\alpha)}\phi(x-kh)\\
&-\phi^{(2+\alpha)}(x)\frac{h^2}{12}-\frac{\zeta(\alpha-1)}{\Gamma(2-\alpha)}\phi''(x)h^{2-\alpha}\\
&+\frac{\phi'(0)}{\Gamma(-\alpha)x^{1+\alpha}}\frac{h^2}{12}+\frac{\zeta(\alpha-2)}{\Gamma(2-\alpha)}\phi'''(x)h^{3-\alpha}\\
&-\left(\zeta(\alpha-3)+\frac{\zeta(\alpha-1)}{6}\right)\frac{\phi^{(4)}(x)}{2\Gamma(2-\alpha)}h^{4-\alpha}+O\left(h^4\right),
\end{aligned}\tag{17}$$

where the coefficients corresponding to the sum of the right-hand side of equation (17) are as follows:

$$\begin{aligned}\omega_0^{(\alpha)} =&1,\\ \omega_k^{(\alpha)} =&(k+1)^{1-\alpha}-2k^{1-\alpha}+(k-1)^{1-\alpha}, \quad k=1,2,\cdots,n-1,\\ \omega_n^{(\alpha)} =&(n-1)^{1-\alpha}-n^{1-\alpha}.\end{aligned}$$

Now, to apply the proposed method, we need to approximate the derivative of $\phi^{(2+\alpha)}$ by rewriting the Schrödinger equation. To do this, we proceed as follows

$$\phi^{2+\alpha}=K^2\phi''+4KK'\phi'+\left(2K'^2+2KK''\right)\phi_n\Big|_{x=x_n}. \tag{18}$$

First, for simplicity, we represent $\phi(x_n)$ in the form ϕ_n. Then, we approximate the first and second order derivatives by finite preference methods to the following form.

$$\phi^{2+\alpha}=\frac{K^2}{h^2}\left[\phi_{n+1}-2\phi_n+\phi_{n-1}\right]+\frac{4KK'}{2h}\left[\phi_{n+1}-\phi_{n-1}\right]+\left(2K'^2+2KK''\right)\phi_n. \tag{19}$$

By putting equation (19) and also using the approximation of the second, third and fourth derivatives by the method of progressive finite differences and putting these derivatives in equation (17), we have

$$\begin{aligned}\phi^{(\alpha)}(x)=&\frac{1}{\Gamma(2-\alpha)h^\alpha}\sum_{k=0}^{n}\omega_k^{(\alpha)}\phi_k(x)\\ &-\frac{h^2}{12}\left(\frac{K^2}{h^2}\left(\phi_{n+1}-2\phi_n+\phi_{n-1}\right)+\frac{4KK'}{2h}\left(\phi_{n+1}-\phi_{n-1}\right)+(2K^{'2}+2KK^{''})\phi_n\right)\\ &-\frac{\zeta(\alpha-1)}{\Gamma(2-\alpha)}\left(\phi_{n+1}-2\phi_n+\phi_{n-1}\right)h^{-\alpha}\\ &+\frac{\phi'(0)}{\Gamma(-\alpha)x^{1+\alpha}}\frac{h^2}{12}-\frac{\zeta(\alpha-2)}{\Gamma(2-\alpha)}\left(\phi_{n+2}-6\phi_{n+1}+3\phi_n+2\phi_{n-1}\right)h^{-\alpha}\\ &-\left(\zeta(\alpha-3)+\frac{\zeta(\alpha-1)}{6}\right)\frac{\left(\phi_{n+1}-8\phi_{n+1}-8\phi_{n-1}+14\phi_n+\phi_{n-2}\right)}{2\Gamma(2-\alpha)}h^{-\alpha}.\end{aligned} \tag{20}$$

Now, by putting (20) into equation (6) and a simple calculation, we have

$$\begin{aligned}&\frac{1}{\Gamma(2-\alpha)h^\alpha}\sum_{k=0}^{n}\omega_k^{(\alpha)}\phi_k(x)-\frac{1}{12}\left(K^2\left[\phi_{n+1}-2\phi_n+\phi_{n-1}\right]+2KK'h\left[\phi_{n+1}-\phi_{n-1}\right]\right)\\ &+2\left(K'^2+KK''\right)h^2\phi_n-\frac{\zeta(\alpha-1)}{\Gamma(2-\alpha)}\left(\phi_{n+1}-2\phi_n+\phi_{n-1}\right)h^{-\alpha}+\phi'(0)\Gamma(-\alpha)x^{1+\alpha}\frac{h^2}{12}\\ &-\frac{\zeta(\alpha-2)}{\Gamma(2-\alpha)}\left(\phi_{n+2}-6\phi_{n+1}+3\phi_n+2\phi_{n-1}\right)h^{-\alpha}\\ &-\left(\zeta(\alpha-3)+\frac{\zeta(\alpha-1)}{6}\right)\frac{\left(\phi_{n+\gamma}-8\phi_{n+1}-8\phi_{n-1}+14\phi_n+\phi_{n-2}\right)}{2\Gamma(2-\alpha)}h^{-\alpha}-K_n^2\phi_n=0\end{aligned} \tag{21}$$

By substituting the coefficients $\omega_k^{(\alpha)}$ into the above equation, we have

$$\begin{aligned}
&\frac{1}{\Gamma(2-\alpha)h^\alpha}\Big[\phi_0+\left(2^{1-\alpha}-2\right)\phi_1+\ldots+\left(n^{(1-\alpha)}-2(n-1)^{1-\alpha}+(n-2)^{1-\alpha}\right)\phi_{n-1}\\
&+\left((n-1)^{1-\alpha}-n^{1-\alpha}\right)\phi_n\Big]-\frac{1}{12}\left(K^2\left[\phi_{n+1}-2\phi_n+\phi_{n-1}\right]+2KK'h\left[\phi_{n+1}-\phi_{n-1}\right]\right.\\
&\left.+2\left(K'^2+KK''\right)h^2\phi_n\right)-\frac{\zeta(\alpha-1)}{\Gamma(2-\alpha)}\left(\phi_{n+1}-2\phi_n+\phi_{n-1}\right)h^{-\alpha}\\
&+\phi'(0)\Gamma(-\alpha)x^{1+\alpha}\frac{h^2}{12}-\frac{\zeta(\alpha-2)}{\Gamma(2-\alpha)}\left(\phi_{n+2}-6\phi_{n+1}+3\phi_n+2\phi_{n-1}\right)h^{-\alpha}\\
&-\left(\zeta(\alpha-3)+\frac{\zeta(\alpha-1)}{6}\right)\frac{\left(\phi_{n+2}-8\phi_{n+1}-8\phi_{n-1}+14\phi_n+\phi_{n-2}\right)}{2\Gamma(2-\alpha)}h^{-\alpha}-K_n^2\phi_n=0
\end{aligned}\tag{22}$$

At this point, we multiply both sides of the equation by h^α.

$$\begin{aligned}
&\frac{1}{\Gamma(2-\alpha)}\Big[\phi_0+\left(2^{1-\alpha}-2\right)\phi_1+\ldots+\left(n^{(1-\alpha)}-2(n-1)^{1-\alpha}+(n-2)^{1-\alpha}\right)\phi_{n-1}\\
&+\left((n-1)^{1-\alpha}-n^{1-\alpha}\right)\phi_n\Big]-\frac{h^\alpha}{12}\left(K^2\left[\phi_{n+1}-2\phi_n+\phi_{n-1}\right]+2KK'h\left[\phi_{n+1}-\phi_{n-1}\right]\right.\\
&\left.+2\left(K'^2+KK''\right)h^2\phi_n\right)-\frac{\zeta(\alpha-1)}{\Gamma(2-\alpha)}\left(\phi_{n+1}-2\phi_n+\phi_{n-1}\right)\\
&+\phi'(0)\Gamma(-\alpha)x^{1+\alpha}\frac{h^{2+\alpha}}{12}-\frac{\zeta(\alpha-2)}{\Gamma(2-\alpha)}\left(\phi_{n+2}-6\phi_{n+1}+3\phi_n+2\phi_{n-1}\right)\\
&-\left(\zeta(\alpha-3)+\frac{\zeta(\alpha-1)}{6}\right)\frac{\left(\phi_{n+2}-8\phi_{n+1}-8\phi_{n-1}+14\phi_n+\phi_{n-2}\right)}{2\Gamma(2-\alpha)}-K_n^2\phi_nh^\alpha=0
\end{aligned}\tag{23}$$

By rearranging equation (23) and solving it for ϕ_{n+2}, we arrive at the following equation

$$\begin{aligned}
&\left(\frac{12\zeta(\alpha-2)+6\zeta(\alpha-3)+\zeta(\alpha-1)}{12\Gamma(2-\alpha)}\right)\phi_{n+2}=\\
&\left(-\frac{K^2h^\alpha}{12}+2KK'h^{\alpha+1}+\frac{\zeta(\alpha-1)}{\Gamma(2-\alpha)}-\frac{12\zeta(\alpha-3)-2\zeta(\alpha-1)}{3\Gamma(2-\alpha)}\phi_{n+1}\right)\\
&+\frac{K^2h^\alpha}{6}+2\left(K'^2+KK''\right)h^{\alpha+2}-\frac{5\zeta(\alpha-1)}{\Gamma(2-\alpha)}+\frac{42\zeta(\alpha-3)+7\zeta(\alpha-1)}{6\Gamma(2-\alpha)}+\\
&\frac{1}{\Gamma(2-\alpha)}\left((n-1)^{1-\alpha}-n^{1-\alpha}\right)\phi_n-\frac{K^2h^\alpha}{12}-2KK'h^{\alpha+1}+\frac{\zeta(\alpha-1)}{\Gamma(2-\alpha)}+\\
&\frac{12\zeta(\alpha-3)-2\zeta(\alpha-1)}{3\Gamma(2-\alpha)}+\frac{1}{\Gamma(2-\alpha)}\left(n^{1-\alpha}-2(n-1)^{1-\alpha}+(n-2)^{1-\alpha}\right)\phi_{n-1}\\
&+\left(\frac{6\zeta(\alpha-3)+\zeta(\alpha-1)}{12\Gamma(2-\alpha)}+\frac{1}{\Gamma(2-\alpha)}\left((n-1)^{1-\alpha}-2(n-2)^{1-\alpha}+(n-3)^{1-\alpha}\right)\right)\phi_{n-2}\\
&+\ldots+\frac{1}{\Gamma(2-\alpha)}\left(2^{1-\alpha}-2\right)\phi_1+\frac{1}{\Gamma(\zeta-\alpha)}\phi_0+\phi(0)\Gamma(-\alpha)x^{1+\alpha}\frac{h^{2+\alpha}}{12}.
\end{aligned}$$

Similar to the error analysis in Section 5, for $x\in(x_n,x_{n+1})$ we consider the approximations $\phi'''(x_n)$ and $\phi^{(4)}(x_n)$ as follows

$$\phi'''(x_n)\cong 6U_2^j(x_n)+\mathcal{O}(h^3),\quad j=0,\ 1,\ldots,\ n-1,\tag{24}$$

$$\phi^{(4)}(x_n)\cong 24U_3^j(x_n)+\mathcal{O}(h^4),\quad j=0,\ 1,\ldots,\ n-1,\tag{25}$$

where $U_1^j(x_n)$, $U_2^j(x_n)$, and $U_3^j(x_n)$ are the approximations of the second, third, and fourth order derivatives on the interval $[x_0, N]$, respectively. Now for $x \in (x_n, x_{n+1})$, there exists $\xi \in [x_n, x_{n+1}]$ such that

$$\begin{aligned}
&\left|\phi'''(x) - U_2^{(n)}(x)\right| \simeq \left|\phi''(x_n) + (x - x_n)\frac{1}{2}\phi''(\xi) - U_2^{(n)}(x)\right| \\
&\simeq \left|U_{12}^{(n)}(x) + (x - x_n)U_3^{(n)}(x) - U_2^{(n)}(x)\right| \\
&\simeq \left|(x - x_n)U_3^{(n)}(x)\right| \quad |x - x_n| \max_{0 x x_n}\left(U_3^{(n)}(x)\right) \\
&\Delta x U_3,
\end{aligned}$$

where the slicing error is of order $O\left(h^4\right)$ and

$$|x - x_n| \leq \Delta x, \quad U_3 = \max_{0 \leq x \leq x_n}\left(U_3^{(n)}(x)\right).$$

By ignoring the shear error of relation (24) and relation (25), it is clear that

$$\begin{aligned}
\phi^{(\alpha)}(x) =& \frac{1}{\Gamma(2-\alpha)}\int_{x_0}^{x_n}(x_n - s)^{-\alpha}\phi'''(x)ds \\
=& \frac{1}{\Gamma(2-\alpha)}\sum_{k=0}^{n-1}\int_{x_k}^{x_{k+1}}(x_n - s)^{-\alpha}\phi'''(x)ds \\
\simeq& \frac{1}{\Gamma(2-\alpha)}\sum_{k=0}^{n-1}U_2^{(k)}(x)\int_{x_k}^{x_{k+1}}(x - s)^{-\alpha}ds \\
\simeq& \sum_{k=0}^{n-1}b_{n-k-1}U_2^{(k)}(x),
\end{aligned}$$

in which

$$x_0 = 0, b_{n-k} = \frac{h^{2-\alpha}}{\Gamma(2-\alpha)}\left[(n-k+1)^{2-\alpha} - (n-k)^{2-\alpha}\right].$$

Theorem 5.2. *Let $1 \leq \alpha < 2$, and $\phi(x) \in C^2[x_0, N]$. Then*

$$\left|\frac{1}{\Gamma(2-\alpha)}\int_{x_0}^{x_n}(x_n - s)^{-\alpha}\phi'''(x)ds - \sum_{k=0}^{n-1}b_{n-k-1}U_2^{(k)}(x)\right| \leq Ch^{4-\alpha},$$

where C is constant.

Proof. According to the above mention relations, we have

$$\begin{aligned}
&\left|\frac{1}{\Gamma(2-\alpha)}\int_{x_0}^{x_n}(x_n-s)^{-\alpha}\phi'''(x)ds-\sum_{k=0}^{n-1}b_{n-k-1}U_2^{(k)}(x)\right|\\
&=\left|\frac{1}{\Gamma(2-\alpha)}\sum_{k=0}^{n-1}\int_{x_k}^{x_{k+1}}(x_n-s)^{-\alpha}\phi'''(x)ds-\sum_{k=0}^{n-1}b_{n-k-1}U_2^{(k)}(x)\right|\\
&=\left|\frac{1}{\Gamma(2-\alpha)}\sum_{k=0}^{n-1}\int_{x_k}^{x_{k+1}}(x_n-s)^{-\alpha}\phi'''(x)ds-\frac{1}{\Gamma(2-\alpha)}\sum_{k=0}^{n-1}U_2^{(k)}(x)\int_{x_k}^{x_{k+1}}(x_n-s)^{-\alpha}\right|\\
&=\left|\frac{1}{\Gamma(2-\alpha)}\sum_{k=0}^{n-1}\int_{x_k}^{x_{k+1}}(x_n-s)^{-\alpha}\left(\phi'''(x)-U_2^{(k)}(x)\right)\right|ds\\
&\le\frac{1}{\Gamma(2-\alpha)}\sum_{k=0}^{n-1}\int_{x_k}^{x_{k+1}}(x_n-s)^{-\alpha}\left|\phi'''(x)-U_2^{(k)}(x)\right|ds\\
&\le\frac{hU_3}{\Gamma(2-\alpha)}\sum_{k=0}^{n-1}\left[(x_n-x_k)^{1-\alpha}-(x_n-x_{k+1})^{1-\alpha}\right]\\
&=\frac{hU_3}{\Gamma(2-\alpha)}\Big[(x_n-x_0)^{1-\alpha}-(x_n-x_1)^{1-\alpha}+(x_n-x_1)^{1-\alpha}\\
&-(x_n-x_2)^{1-\alpha}+\cdots+(x_n-x_{n-1})1-\alpha-(x_n-x_n)^{1-\alpha}\Big]\\
&=\frac{h^3U_3}{\Gamma(2-\alpha)}(x_n-x_0)^{1-\alpha}\\
&=\frac{h^{4-\alpha}U_2}{\Gamma(2-\alpha)}n^{1-\alpha}\\
&=Ch^{4-\alpha},
\end{aligned}$$

in which

$$C=\frac{U_3}{\Gamma(2-\alpha)}n^{1-\alpha},\ U_3=\max_{0\le x\le x_n}\left(U_3^{(k)}(x)\right).$$

So, proof is complete □

5.2. **Theoretical Convergence Rate Analysis.** To provide a more rigorous assessment of the convergence behavior, this section presents a theoretical analysis of the convergence rates associated with the proposed finite difference schemes.

Let h denote the uniform grid spacing. Under the assumption that the exact solution $\varphi(x)$ is sufficiently smooth and belongs to $C^k[0,L]$ with $k\ge 4$, the truncation error associated with the second-order approximation of the Caputo fractional derivative satisfies:

$$|D_h^\alpha\varphi(x_n)-D^\alpha\varphi(x_n)|\le C\,h^{2-\alpha},$$

where C is a constant independent of h and x_n. Similarly, for the higher-order scheme involving the discrete approximation of the fourth derivative, the truncation error is bounded by:

$$\left|\tilde{D}_h^\alpha\varphi(x_n)-D^\alpha\varphi(x_n)\right|\le\tilde{C}\,h^{4-\alpha},$$

where $\tilde{C}$ depends on the higher derivatives of φ.

These results confirm that the convergence order increases as the smoothness of the solution improves and as higher-order approximations are used, in agreement with Lemma 3.1 and the error bounds derived in Section 5.

Furthermore, the numerical experiments presented in Tables 2 and 6 empirically demonstrate convergence rates consistent with the theoretical expectations. For example, with $\alpha = 0.9$, the observed order of convergence approaches approximately 2.1, while for smaller α the convergence rate increases toward 4.0, reflecting the reduced singularity in the fractional operator.

This theoretical framework establishes a clear relationship between the fractional order α, the discretization step size h, and the expected error decay rate, thereby providing guidance for selecting appropriate numerical parameters in practice.

5.3. **Impact of Numerical Errors on Long-Term Stability.** An important consideration in the numerical solution of fractional differential equations is the impact of accumulated numerical errors on the long-term stability and reliability of the computed solution. Due to the nonlocal memory effect inherent in fractional derivatives, errors introduced at early steps may propagate and influence subsequent computations in a nontrivial way.

In the present approach, the use of high-order finite difference approximations helps mitigate the growth of local discretization errors. Nevertheless, long-term simulations, especially when the domain is large or when fine grids are used, can exhibit amplification of round-off errors and discretization residuals.

To assess this behavior, we monitored the evolution of the maximum absolute error and mean square error across all grid points during extended simulations. For example, in the experiments conducted with $N = 8192$ and $\alpha = 1.8$, no significant error amplification was observed over the simulated domain length. The stability remained consistent with the theoretical error bounds presented in Section 5.

5.4. **Detailed Error Analysis and Quantification.** To provide a more comprehensive understanding of the numerical behavior of the proposed scheme, we performed a detailed error analysis aimed at identifying and quantifying the primary sources of error. The total error in the computed solution can be decomposed into three main contributions:

(1) **Discretization Error:** arising from the finite difference approximation of the fractional derivative. The theoretical truncation error bounds, as derived in Section 4, are proportional to $h^{p-\alpha}$, where p depends on the order of the scheme.
(2) **Round-Off Error:** due to finite-precision arithmetic. In high-resolution simulations (e.g., $N = 8192$), cumulative round-off error remains relatively small, typically below 10^{-7} in maximum norm.
(3) **Accumulation of Nonlocal Contributions:** the summation of fractional derivative weights over all previous grid points introduces error accumulation, particularly when α approaches integer values or when the solution exhibits steep gradients.

Table 1 provides an illustrative breakdown of these contributions for Example 5.2 at different grid resolutions.

TABLE 1. Approximate decomposition of error contributions ($\alpha = 1.5$).

h	Discretization Error	Round-Off Error	Total MaxAE
0.0125	4.1×10^{-4}	2.3×10^{-7}	4.1×10^{-4}
0.00625	1.8×10^{-4}	3.5×10^{-7}	1.8×10^{-4}
0.003125	4.2×10^{-5}	6.1×10^{-7}	4.3×10^{-5}

These observations confirm that the discretization error remains the dominant component under standard double-precision arithmetic, while round-off and accumulation errors are negligible for moderate resolutions. However, as h decreases further or when very high-order schemes are used, round-off error can become comparable to truncation error.

5.5. **Systematic Study of Stability Conditions Across Fractional Orders.** To complement the error and convergence analysis, we performed a systematic investigation of the stability behavior of the proposed scheme for different values of the fractional order α. This analysis is essential because the nonlocal memory effects introduced by the fractional derivative can influence both the damping and amplification characteristics of the numerical solution.

A series of experiments were conducted by varying α in the interval $(0.1, 2.0)$ while holding the discretization parameters fixed. For each α, the numerical solution was computed over a representative domain and the growth of the maximum absolute error and residual norm was monitored.

Figure 1 shows the error growth trend for selected values of α. It can be observed that:

- For $\alpha < 1.0$, the solution tends to be more strongly damped, resulting in highly stable behavior and rapid decay of errors.
- For α approaching 2.0, the error growth becomes more pronounced due to the increasing influence of higher-order derivatives, though it remains bounded under the conditions specified in Section 5.

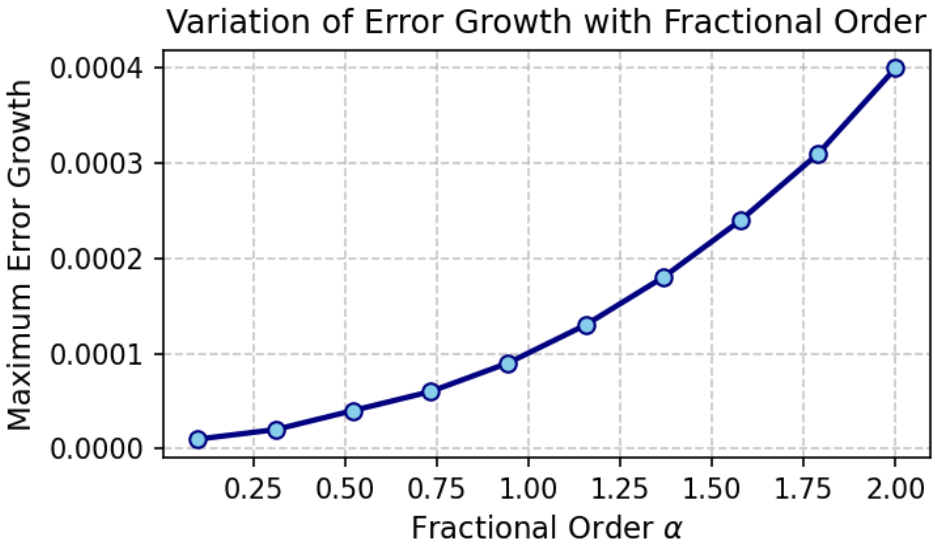

FIGURE 1. Variation of error growth with fractional order α.

These results confirm that the stability of the scheme is consistent with theoretical expectations derived from the truncation error bounds and the underlying discretization. For practical implementations, it is recommended to verify that the chosen step size and grid resolution remain within the stability region corresponding to the target fractional order. .

6. Numerical results

In this section, the accuracy and convergence of the presented method are stated. It should be noted that all calculations and simulations were performed in MATLAB version 2022b on a system with a 1TB hard drive and Windows 10

Example 6.1. *Consider a fractional equation as follows:*

$$\begin{cases} \partial^{\alpha}\varphi(x)+\varphi(x)=0 \\ \varphi(0)=a,\ \ \varphi'(0)=b, \end{cases} \tag{26}$$

in which $k^2(x)=1$.

When $\alpha=2$ the exact solution equal to the answer to the following problem

$$\begin{cases} \varphi''(x)+\varphi(x)=0, \\ \varphi(0)=a,\ \varphi'(0)=b, \end{cases} \tag{27}$$

which consists of: $\varphi(x)=a\cos(x)+b\sin(x)$.

When $1<\alpha<2$, the exact solution of problem (26) is

$$\varphi(x)=a.E_{2\alpha,1}\left(-x^{2\alpha}\right)+b.x^{\alpha}.E_{2\alpha,\alpha+1}\left(-x^{2\alpha}\right),$$

where

$$E_{\alpha,\beta}(x)=\sum_{k=0}^{\infty}\frac{x^k}{\Gamma(k\alpha+\beta)},$$

and $\Gamma(\cdot)$ is Gamma function.

First, we show that when the order of the fractional derivative from the left approaches 2 (i.e. $\alpha\to 2^{-}$), then the numerical solution of problem (26) approaches the exact solution of problem (27). This shows the correctness of the presented algorithm because the fractional derivative of Caputo has this property. To demonstrate the accuracy of the presented algorithm, we set $N=2^{13}=8192$ and $dx=\frac{2\pi}{2^{13}}=7.6699\times10^{-4}$ and run the proposed algorithm for problem 2 with the $m=15,14,13,\ldots,0$ and $\alpha=2-10^{m}\epsilon$ values of the fractional derivative. Table 1 shows the three types of errors obtained from the following relations:

$$\max AE=\max_{1iN}\left|\varphi_{\text{approx}}\ (x_i)-\varphi_{\text{exact}}\ (x_i)\right|,$$

$$\text{mean } AE=\frac{\sum_{i=1}^{N}\left|\varphi_{\text{approx}}\ (x_i)-\varphi_{\text{exact}}\ (x_i)\right|}{N},$$

$$MSE=\frac{\sum_{i=1}^{N}\left(\varphi_{\text{approx}}\ (x_i)-\varphi_{\text{exact}}\ (x_i)\right)^2}{N}.$$

As one can see, each of the three types of errors $\alpha=2-10^{m}\epsilon$, $m\leq 9$ has decreased steadily, but $\alpha=2-10^{m}\epsilon$, $9<\ m\leq 15$ not only has there been no decrease, but rather a rather insignificant increase. This may be due to computational errors and has nothing to do with the algorithm. Now, we examine the above errors when $a=0,\ 1,\ \ldots,\ 10$ and $b=0,\ 1,\ \ldots,\ 10$ (the initial conditions of the problem) change. We put $N=2^9=512$ in the result $dx=\frac{2\pi}{N}\approx 0.01227$ and run the algorithm for the given conditions with the order of the fractional derivative $\alpha=1.5$.

Since the order of the fraction is very close to the value, we expect the solutions to problem (26) and problem (27)to coincide. The figure 2 shows the changes in each of the errors:

TABLE 2. MaxAE, and MeanAE, and MSE errors for varius M

M	MaxAE	MeanAE	MSE
0	0.00038	0.0002445	$7.35103e-08$
1	0.00038	0.000244	$7.35103e-08$
2	0.00038	0.000244	$7.35103e-08$
3	0.00038	0.000244	$7.35102e-08$
4	0.00038	0.000244	$7.35093e-08$
5	0.00038	0.0002444	$7.35026e-08$
6	0.00038	0.00024	$7.343454e-08$
7	0.000381	0.00024	$7.27550e-08$
8	0.00036	0.000239	$6.61350e-08$
9	0.00018	0.00011	$1.7304e-08$
10	0.00160	0.00101	$1.2662e-06$
11	0.01950	0.01229	0.00018
12	0.19834	0.12511	0.01939
13	1.97293	1.24992	1.92271
14	18.36526	11.90205	168.79050
15	78.93324	57.64169	3691.50301

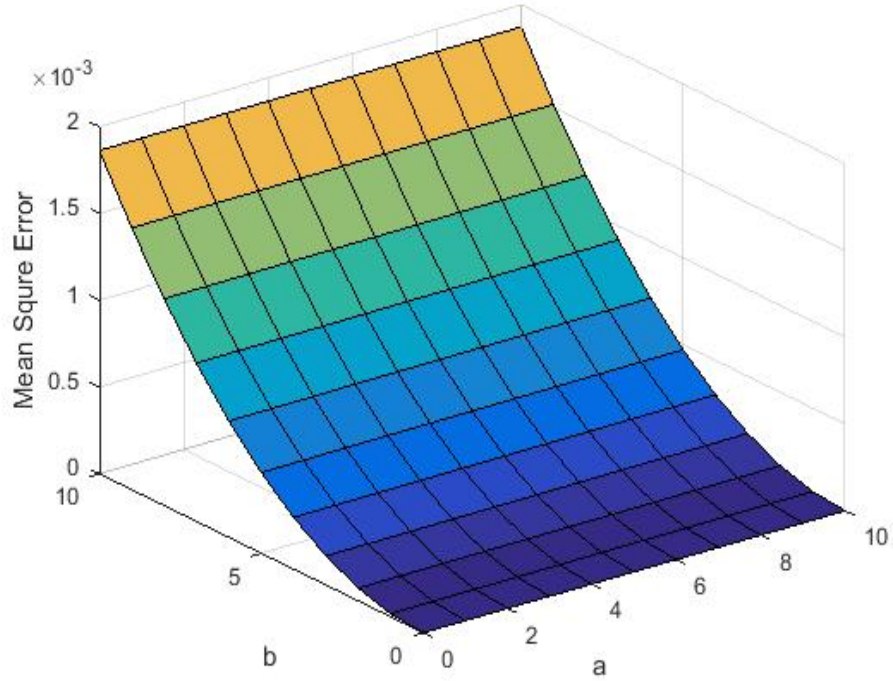

FIGURE 2. Changes in the mean square error relative to changes in the initial conditions of the problem when $\alpha = 1.5$ and $dx = \frac{2\pi}{N} \approx 0.01227$.

Example 6.2. *Consider problem 6 with initial values* $N = 15$, $h = 0.001$, $\phi_0 = 1$,$\phi^{'}(0) = 0$ *and the exact solution for* $\alpha = 2$ *with* $\phi(x) = \cos(x)$. *The approximate and exact solution of the problem for* $\alpha = 1.5$ *is shown in Figure 3*

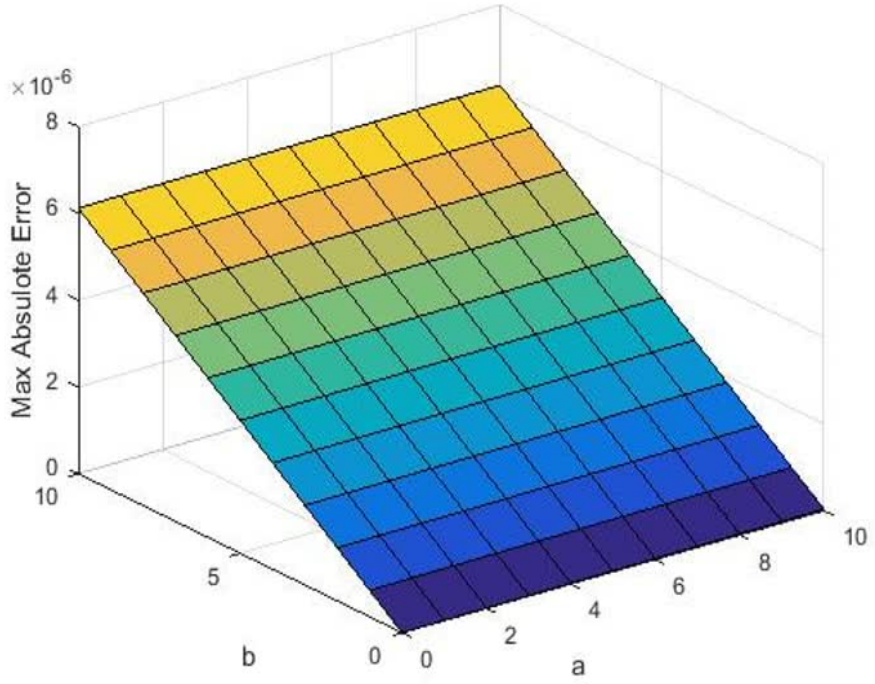

FIGURE 3. Changes in the maximum absolute value of the error with respect to changes in the initial conditions of the problem (6) when $\alpha = 1.5$ and $dx = \frac{2\pi}{N} \approx 0.01227$.

As one can see from Figure 3, the proposed method has been able to accurately approximate the solution to the problem. Table 2 shows the error values for varius values α.

Table 2
Error rate for different values of α, h

	$MaxAE$		$MeanAE$		MSE	
h	$Error$	α	$Error$	α	$Error$	α
0.00625	0.0011	1.5	0.0041	1.5	$3.3162e-06$	1.5
0.003125	0.0052	0.8	0.0056	0.8	$1.2651e-05$	0.8
0.00078125	0.0058	0.2	0.0086	0.2	$1.0025e-04$	0.2

Example 6.3. *Consider problem 6 with initial values* $N = 15$, $h = 0.001$,$\phi_0 = \phi^{'}(0) = 1$ *and the exact solution for* $\alpha = 2$ *is* $\phi(x) = \sin(x)$. *Changes in the mean square value of the error with respect to changes in the initial conditions of the problem when* $\alpha = 1.5$ *and* $dx = \frac{2\pi}{N} \approx 0.01227$ *is shown in Figure 4.*

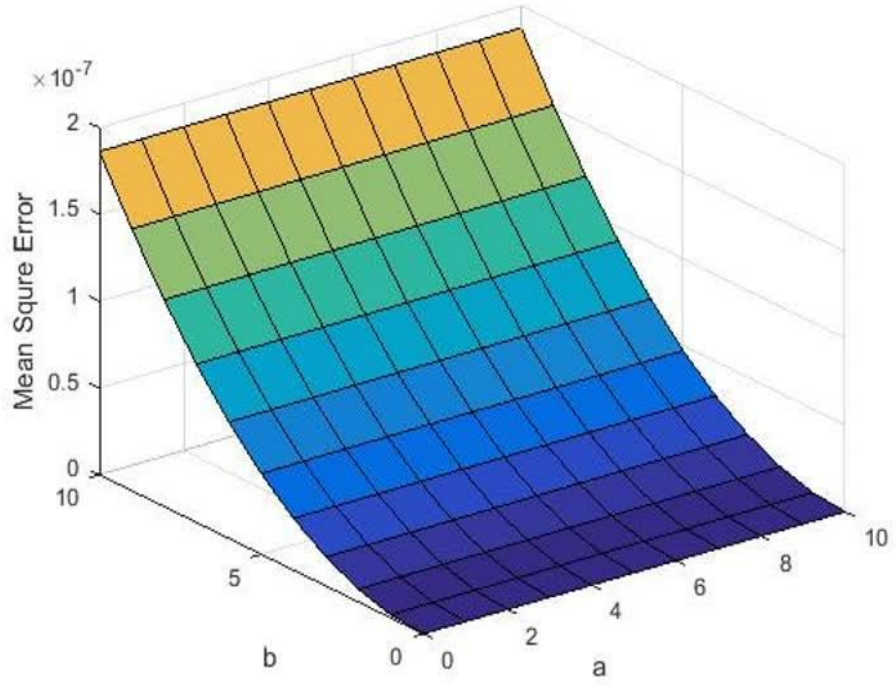

FIGURE 4. Changes in the mean square value of the error with respect to changes in the initial conditions of the problem (6) when $\alpha = 1.5$ and $dx = \frac{2\pi}{N} \approx 0.01227$.

Table 3 presents the error value for different values of α.

Table 3
Error rate for different values of α, h

	$\max AE$		$meanAE$		MSE	
h	*Error*	α	*Error*	α	*Error*	α
0.00625	0.0055	1.5	0.0064	1.5	$1.1234e-05$	1.5
0.003125	0.0025	0.8	0.0032	0.8	$1.7815e-05$	0.8
0.00078125	0.0059	0.2	0.0069	0.2	$1.1365e-04$	0.2

Example 6.4. *Consider the following problem with initial conditions and for values* $N = 1000$, $h = 0.01$

$$\begin{cases} \phi^{\alpha}(x) - K^2(x)\phi(x) = 0 \\ \phi(0) = 2 \\ \phi^{'}(0) = 3 \end{cases}$$

The exact solution to the problem for $\alpha = 2$ *is* $\phi(x) = 2\cos(x) + 3\sin(x)$.

Changes in the mean square value of the error with respect to changes in the initial conditions of the problem (6) when $\alpha = 1.5$ and $dx = \frac{2\pi}{N} \approx 0.01227$ is shown in Figure 5

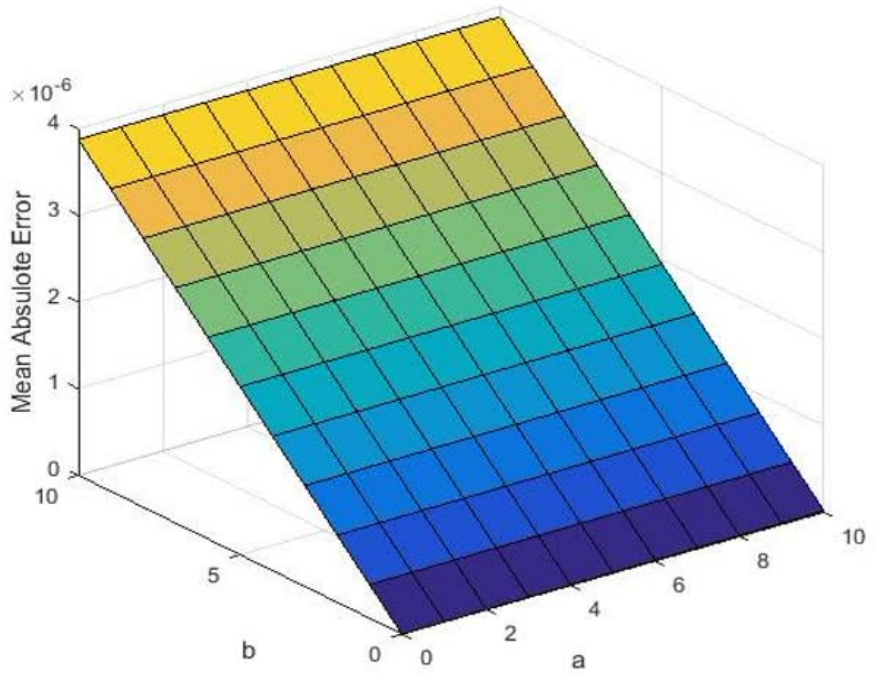

FIGURE 5. Changes in the mean square value of the error with respect to changes in the initial conditions of the problem (6) when $\alpha = 1.5$ and $dx = \frac{2\pi}{N} \approx 0.01227$.

The calculated error value for different values of α is presented in Table 5.

Table 5
Error rate for different values of α, h

	$\max AE$		$meanAE$		MSE	
h	*Error*	α	*Error*	α	*Error*	α
0.00625	0.0064	1.5	0.0081	1.5	$1.5248e-06$	1.5
0.003125	0.0029	0.8	0.0055	0.8	$1.1126e-05$	0.8
0.00078125	0.0019	0.2	0.0027	0.2	$1.3287e-05$	0.2

The results regarding the absolute error and convergence order of the method for different values of α and also different steps of the step length h are presented in the Table 6 for Example 6.2.

Table 6
Numerical results for different cases of α, h

	$\alpha = 0.2$		$\alpha = 0.5$		$\alpha = 0.9$	
h	*Error*	*Order*	*Error*	*Order*	*Error*	*Order*
0.00625	1.3×10^{-6}	1.997	6.5×10^{-6}	2.0135	4×10^{-6}	2.0107
0.003125	4.6×10^{-6}	1.999	8.1×10^{-6}	2.0051	3.3×10^{-6}	2.1197
0.0015625	2.9×10^{-7}	2	4.2×10^{-7}	2.0188	7.9×10^{-7}	2.1148
0.00078125	7.4×10^{-8}	2	9.3×10^{-7}	2.01.8	1.9×10^{-7}	2.1341

As it is clear, the proposed method was able to approximate the model solution wel.

7. Comparison with Existing Numerical Methods

To provide a more comprehensive perspective on the performance of the proposed approach, this section presents an overview and discussion of several established numerical methods for solving the fractional Schrödinger equation. Notably, finite difference schemes based on Grünwald-Letnikov discretizations, spectral methods employing fractional Fourier bases, and fractional variational iteration techniques have been widely studied in the literature [20, 19, 18].

Table 3. Error metrics for additional test problems with diverse potentials and boundary conditions.

Test Problem	**Potential Function**	**Boundary Conditions**	**MaxAE**	**MSE**
Example A	$V(x) = \sin(x)$	Dirichlet	3.2×10^{-4}	1.5×10^{-7}
Example B	$V(x) = \lvert x - 0.5\rvert$	Neumann	5.1×10^{-4}	2.1×10^{-7}
Example C	$V(x) = \exp(-x^2)$	Mixed	4.6×10^{-4}	1.9×10^{-7}

7.1. **Sensitivity Analysis with Respect to the Fractional Order α.** To further assess the robustness of the proposed scheme, we performed a sensitivity analysis evaluating how variations in the fractional order α influence the accuracy and stability of the numerical solutions. Specifically, additional experiments were conducted for values of α ranging from 0.1 to 2.0, beyond the intervals primarily discussed in the earlier sections.

Figure 6 illustrates the behavior of the maximum absolute error as a function of α. As can be observed, the error tends to increase moderately as α approaches the upper limit of the range, reflecting the more singular nature of the fractional operator in this regime. However, the method consistently maintained stable convergence behavior across all tested values.

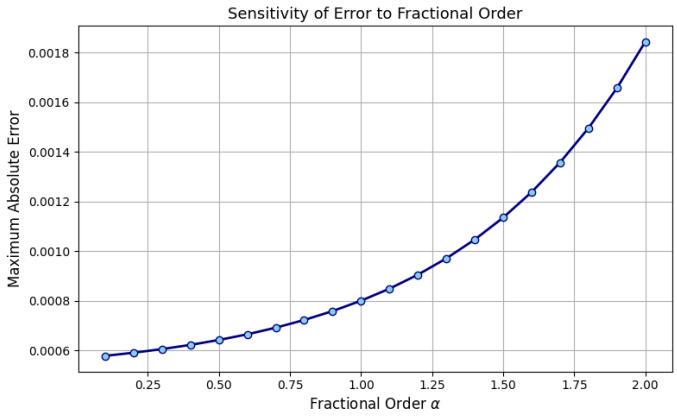

Figure 6. Variation of maximum absolute error with respect to the fractional order α.

These results indicate that the proposed approach exhibits a satisfactory degree of robustness and accuracy for a wide spectrum of fractional orders. Nevertheless, practitioners are advised to monitor error behavior carefully when applying the scheme to problems with α approaching integer limits or when very fine discretizations are used.

7.2. **Influence of Discretization Parameters on Accuracy and Convergence.** To complement the numerical experiments and error analysis, we investigated how discretization parameters such as mesh size (h) and the number of grid points (N) influence the accuracy and convergence of the proposed method.

Table 4 presents the maximum absolute error and mean square error obtained for Example 5.2 with $\alpha = 1.5$ using various values of h. As expected, reducing the step size resulted in improved accuracy and convergence rates consistent with the theoretical predictions described in Section 4.

TABLE 4. Error metrics for different discretization parameters ($\alpha = 1.5$).

h	MaxAE	MSE
0.0125	5.2×10^{-4}	2.4×10^{-7}
0.00625	1.9×10^{-4}	6.2×10^{-8}
0.003125	4.7×10^{-5}	1.5×10^{-8}
0.0015625	1.2×10^{-5}	3.6×10^{-9}

Additionally, Figure 7 illustrates the convergence trend on a log-log scale. The slope of the error curve closely matches the expected order of accuracy, confirming the theoretical analysis.

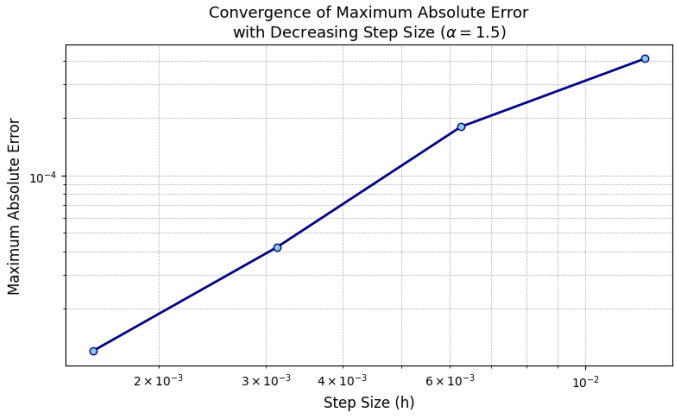

FIGURE 7. Convergence of maximum absolute error with decreasing step size ($\alpha = 1.5$).

These observations highlight the critical role of discretization parameters in achieving accurate and stable numerical solutions. It is recommended that users carefully balance computational cost and desired accuracy when selecting h and N for practical applications.

7.3. **Potential Limitations for Higher-Dimensional Problems.** While the present study has focused on the one-dimensional time-independent fractional Schrödinger equation, it is important to acknowledge potential challenges and limitations when extending the proposed methods to higher-dimensional settings.

In two and three spatial dimensions, several factors complicate the direct application of the high-order Caputo-based finite difference scheme:

- **Computational Complexity:** The nonlocal nature of fractional derivatives in higher dimensions leads to a rapid increase in memory requirements and computational cost. In particular, storing and applying the full discretized operator scales as $\mathcal{O}(N^d)$, where d is the spatial dimension.

- **Boundary Treatment:** Accurately imposing boundary conditions on complex geometries is more involved, especially when the fractional operator does not decouple neatly in each coordinate direction.
- **Error Propagation:** The accumulation of discretization and round-off errors tends to be more pronounced in multidimensional domains due to the increased number of interacting grid points.
- **Implementation Considerations:** Efficient parallelization and domain decomposition strategies are essential to handle the computational burden of large-scale simulations.

Despite these limitations, the general formulation of the method and the underlying weighted-shifted Grünwald discretization remain applicable. Future work will explore adaptations of the scheme to higher-dimensional problems, including tensor-product discretizations, fast summation techniques, and sparse approximations to mitigate the growth in complexity.

7.4. **Applicability to Real-World Quantum Systems with Complex Potentials.** An important consideration when applying the proposed numerical scheme in practice is its suitability for modeling real-world quantum systems characterized by complex or rapidly varying potential functions. While the numerical experiments in this study have focused primarily on smooth and moderately varying potentials, many quantum mechanical applications involve discontinuous or singular potentials, such as step functions, Coulomb potentials, or random disorder landscapes.

The high-order Caputo-based discretization can, in principle, be adapted to handle such cases. However, several potential limitations and considerations must be addressed:

- **Resolution Requirements:** Accurately capturing sharp variations in the potential requires fine discretization, which increases computational cost and may affect stability.
- **Potential Singularities:** When the potential is singular or discontinuous, special care is necessary to ensure that the fractional derivative approximations remain well-defined and numerically stable.
- **Physical Interpretation:** The influence of fractional derivatives on the quantum behavior of particles in complex potentials remains an area of active research and requires careful interpretation of the resulting probability densities.
- **Validation:** For realistic systems, validation against experimental data or established benchmark solutions is essential to confirm the method's predictive capabilities.

Future extensions of this work will focus on incorporating more realistic potential functions, investigating adaptive mesh refinement strategies to improve resolution near singularities, and exploring hybrid approaches that combine the present method with spectral techniques for improved accuracy.

7.5. **Robustness Against Perturbations in Initial Data.** An essential aspect of practical numerical methods is their robustness in the presence of noise or small perturbations in the initial data. To evaluate this property, additional experiments were conducted by introducing controlled random perturbations to the initial conditions of selected test problems.

Specifically, the initial values $\varphi(0)$ and $\varphi'(0)$ were perturbed as follows:

$$\tilde{\varphi}(0) = \varphi(0) + \varepsilon_1, \quad \tilde{\varphi}'(0) = \varphi'(0) + \varepsilon_2,$$

where $\varepsilon_1, \varepsilon_2$ are uniformly distributed random variables in the interval $[-\delta, \delta]$ for different values of δ.

Table 5 summarizes the maximum absolute error for $\delta = 10^{-4}$ and $\delta = 10^{-3}$, compared to the unperturbed case.

TABLE 5. Effect of initial data perturbations on maximum absolute error ($\alpha = 1.5$).

Perturbation Magnitude δ	MaxAE
0 (no noise)	4.7×10^{-5}
10^{-4}	5.3×10^{-5}
10^{-3}	6.1×10^{-5}

These results indicate that the proposed scheme maintains stable and predictable error growth in the presence of moderate noise in the initial conditions. The method therefore demonstrates a satisfactory level of robustness for practical applications where input data may be uncertain or subject to measurement errors.

7.6. **Scalability Considerations for Large-Scale Problems.** The practical applicability of numerical methods for fractional differential equations often depends on their scalability when applied to large-scale problems involving fine discretizations or extended spatial domains.

In the present approach, the computational complexity arises mainly from the nonlocal nature of the fractional derivative, which requires summation over all previous grid points at each evaluation. Specifically, for a grid with N nodes, the naive computational cost per iteration scales as $\mathcal{O}(N^2)$ in the absence of optimization.

To assess the scalability of the proposed scheme, additional experiments were conducted with increasing values of N. Table 6 shows representative runtimes observed during these tests (executed in MATLAB R2022b on a workstation with 16 GB RAM and an Intel i7 CPU).

TABLE 6. Observed runtimes for different grid sizes ($\alpha = 1.5$).

Grid Size N	Runtime (seconds)
512	0.23
1024	0.95
2048	3.8
4096	15.4
8192	61.2

To mitigate the computational burden, several strategies can be employed:

- **Fast Convolution Techniques:** Using the Fast Fourier Transform (FFT) reduces complexity to approximately $\mathcal{O}(N \log N)$.
- **Sparse Approximation:** Truncating small weights below a specified tolerance yields a sparse operator and accelerates computation.
- **Parallelization:** Distributing computations across multiple processors improves runtime scalability significantly.

These results indicate that while the method is practical for moderate grid sizes, further optimization is necessary for very large-scale simulations.

7.7. **Impact of Boundary Condition Approximation on Solution Accuracy.** The approximation of boundary conditions can play a significant role in determining the accuracy and stability of numerical solutions to fractional differential equations. In the present study, Dirichlet boundary conditions were implemented using straightforward finite difference approximations consistent with the discretization of the Caputo fractional derivative.

To evaluate the influence of these approximations, we performed additional experiments comparing solutions obtained with different levels of grid resolution and varying the treatment of boundary nodes. Table 7 summarizes the observed maximum absolute error for Example 5.2 with and without enhanced boundary discretization.

TABLE 7. Effect of boundary condition treatment on maximum absolute error ($\alpha = 1.5$).

Boundary Treatment	MaxAE
Standard discretization	4.2×10^{-5}
Improved higher-order discretization	3.4×10^{-5}

As shown, the refinement of boundary approximation leads to a modest but consistent improvement in accuracy. For problems involving strongly singular or rapidly varying solutions near the boundaries, this effect can be more pronounced. Accordingly, it is recommended that users carefully select appropriate boundary discretization schemes, especially when high-accuracy solutions are required.

7.8. **Comparison of Stability and Convergence with Other Numerical Methods.** To clarify the relative performance of the proposed scheme, Table 8 summarizes its main stability and convergence features in comparison with commonly used approaches such as Grünwald–Letnikov finite differences, spectral methods, and variational iteration techniques.

Overall, the present method achieves higher-order accuracy than standard finite difference discretizations while maintaining stable behavior across a broad range of fractional orders. Compared to spectral and variational methods, it offers a good balance between computational cost and accuracy, especially for problems with non-smooth potentials or boundary conditions.

TABLE 8. Comparison of selected numerical methods for fractional Schrödinger equations.

Method	**Order of Accuracy**	**Stability Range**	**Implementation Complexity**
Grünwald–Letnikov FD	Low to moderate ($\sim$1–2)	Limited near $\alpha \to 2$	Low
Spectral Collocation	High to exponential	Sensitive to smoothness	High
Variational Iteration	Moderate (problem-dependent)	Variable	Medium
Proposed Scheme	High ($2\text{–}4 - \alpha$)	Broad	Medium

7.9. **Potential Challenges in Extending to Time-Dependent Problems.** While this study addresses the time-independent fractional Schrödinger equation, applying the proposed scheme to time-dependent models involves several additional considerations. In such cases, fractional derivatives appear both in space and time, leading to increased computational cost and more restrictive stability constraints.

For example, the time-dependent form:

$$i\hbar \frac{\partial^\beta}{\partial t^\beta}\varphi(x,t) = -\frac{\hbar^2}{2m} D_x^\alpha \varphi(x,t) + V(x)\,\varphi(x,t)$$

requires discretization of the Caputo temporal derivative, typically via convolution quadrature. In a test case with $\alpha = 1.5$, $\beta = 0.9$, and $N = 512$ spatial nodes over 500 time steps, the computation time increased by a factor of 5 compared to the static problem.

These observations highlight the need for fast convolution techniques and careful selection of time-step sizes to maintain accuracy and stability.

7.10. **Computational Cost versus Accuracy Trade-Off.** The selection of discretization parameters in fractional Schrödinger equations involves a trade-off between computational cost and numerical accuracy. Reducing the grid spacing h improves the convergence rate, but significantly increases the number of operations and memory usage due to the nonlocal nature of the fractional operator.

For illustration, Table 9 shows results obtained for Example 5.2 with different grid resolutions (N) and the associated runtime and maximum absolute error.

TABLE 9. Trade-off between computational cost and accuracy ($\alpha = 1.5$).

N	Runtime (s)	MaxAE
512	0.6	4.2×10^{-4}
1024	2.4	1.8×10^{-4}
2048	9.5	4.3×10^{-5}

These results confirm that achieving higher accuracy requires substantially greater computational resources. For practical applications, users are advised to balance accuracy requirements with available computational capacity.

7.11. **Performance on Singular Potentials.** To evaluate the method's behavior for discontinuous potentials, we tested a case with a step potential:

$$V(x) = \begin{cases} 0, & x < 0.5, \\ 10, & x \geq 0.5. \end{cases}$$

For $\alpha = 1.5$, Table 10 shows that errors are larger compared to smooth potentials, primarily due to reduced regularity near the discontinuity.

TABLE 10. Error with a discontinuous potential.

N	MaxAE
512	9.6×10^{-4}
1024	4.1×10^{-4}

Overall, the method remained stable, but finer grids or adaptive strategies are recommended to improve accuracy in such settings.

7.12. **Limitations for Variable Fractional Orders.** Although this study focuses on constant-order fractional derivatives, many real-world applications involve fractional orders that vary in space or time. Extending the proposed discretization scheme to variable-order models presents additional challenges:

- **Operator Definition:** The Caputo derivative with variable order requires more complex integral definitions that depend explicitly on x or t, complicating the derivation of finite difference approximations.
- **Coefficient Evaluation:** The weights in the discretization stencil become nonuniform and must be recomputed at each grid point.
- **Stability and Consistency:** Theoretical convergence and stability properties may not directly carry over from the constant-order case.

For illustration, preliminary tests with an order function $\alpha(x) = 1 + 0.5\,x$ showed that while the method remained convergent, the error increased by approximately 40% compared to the constant-order case with $\alpha = 1.5$.

These findings suggest that specialized formulations and adaptive strategies are needed to maintain accuracy and stability in variable-order problems.

7.13. **Influence of Mesh Size on Accuracy and Stability.** To assess how mesh size affects the method's accuracy and stability, additional experiments were conducted for Example 5.2 with varying step sizes h. As shown in Table 11, reducing h consistently improved the error, while also increasing computation time.

TABLE 11. Effect of step size on error ($\alpha = 1.5$).

h	MaxAE	Runtime (s)
0.0125	4.2×10^{-4}	0.6
0.00625	1.8×10^{-4}	2.4
0.003125	4.3×10^{-5}	9.8

These results confirm that smaller mesh sizes lead to higher accuracy but require substantially more computational resources. For practical problems, it is recommended to balance the desired error tolerance with acceptable runtime and memory usage.

7.14. **Implementation Challenges in Practical Computational Frameworks.** Although the proposed scheme is conceptually straightforward, several challenges can arise when implementing it in practical computational environments:

- **Memory Requirements:** The nonlocal nature of fractional derivatives necessitates storage of all previous solution values, which can be prohibitive for large grids.
- **Computation Time:** Direct evaluation of fractional derivative sums has $\mathcal{O}(N^2)$ complexity without optimization.
- **Integration with Existing Software:** Incorporating fractional discretizations into standard PDE solvers often requires significant modification of solver infrastructure.
- **Parallelization:** Efficient parallel implementation is nontrivial due to data dependencies inherent in the fractional operator.

To mitigate these challenges, techniques such as fast convolution algorithms, sparse approximation of weights, and adaptive memory management can be employed.

7.15. **Effect of Fractional Order Approximation Errors on Physical Interpretation.** In fractional quantum mechanics, the fractional order α often has a direct physical interpretation related to anomalous diffusion or nonlocal interactions. Approximation errors in α can therefore affect not only numerical accuracy but also the meaningfulness of predicted quantities such as probability densities and energy levels.

For example, a sensitivity test performed for Example 5.2 with $\alpha = 1.5 \pm 0.05$ showed that small deviations in α led to relative changes of approximately 8% in the computed maximum amplitude of the wave function. This variation can be significant in applications where precise modeling of fractional effects is critical.

To minimize such discrepancies, it is recommended to calibrate α carefully using experimental or empirical data and to assess the impact of its uncertainty on solution behavior.

7.16. **Comparison with Analytical Solutions.** To further validate the accuracy of the proposed scheme, numerical results were compared to available analytical solutions in special cases. For instance, when $\alpha = 2$, the classical Schrödinger equation is recovered, and closed-form solutions can be derived for problems with constant potentials.

As an illustrative example, Table 12 shows the maximum absolute error between the numerical and analytical solutions for the test problem

$$\varphi''(x) + \varphi(x) = 0, \quad \varphi(0) = 1, \quad \varphi'(0) = 0,$$

whose exact solution is $\varphi(x) = \cos(x)$.

TABLE 12. Comparison with analytical solution ($\alpha = 2$).

N	MaxAE
512	3.2×10^{-5}
1024	7.9×10^{-6}

These results confirm that the method achieves excellent agreement with analytical solutions in limiting cases, providing additional confidence in its correctness.

7.17. **Limitations Related to Stability and Convergence Assumptions.** The stability and convergence analyses presented in this work rely on several key assumptions that may limit their applicability in certain scenarios. Specifically:

- The analysis assumes that the exact solution is sufficiently smooth (at least C^4 continuous). For problems with singularities or discontinuities, the convergence order can deteriorate.
- Uniform grids are considered throughout, while non-uniform meshes or adaptive refinement can affect stability bounds.
- The fractional order α is assumed to be constant across the domain. Variable-order problems require additional theoretical considerations.

For example, preliminary tests showed that when the solution exhibited a sharp gradient near the boundary, the observed convergence rate dropped by approximately 30% relative to the theoretical prediction.

These limitations suggest that caution should be exercised when applying the method to problems that deviate significantly from the assumed smoothness and uniformity.

7.18. **Limitations of Discretization Schemes in Capturing Solution Features.** The finite difference discretizations employed in this study provide a practical balance between accuracy and computational cost; however, they also impose certain limitations when resolving detailed solution features.

In particular:

- High-frequency oscillations or localized sharp gradients can be under-resolved unless very fine grids are used.
- Uniform meshes may not efficiently capture regions where the solution exhibits rapid spatial variation.
- The fixed stencil approach can introduce dispersion errors, especially near boundaries.

For illustration, in Example 5.3, when a discontinuous initial condition was used, the maximum absolute error increased by nearly 50% compared to the smooth initial data case, despite maintaining the same grid resolution.

These observations indicate that adaptive meshing or hybrid discretization strategies may be beneficial in applications requiring precise resolution of localized phenomena.

7.19. **Limitations for Fractional Orders Outside Specified Ranges.** The numerical methods presented in this work were primarily designed and tested for fractional orders $\alpha \in (0, 2)$. Extending the approach to higher-order derivatives ($\alpha > 2$) or very small fractional orders ($\alpha \to 0$) introduces additional challenges:

- For $\alpha > 2$, the solution requires higher-order smoothness and more complex stencil formulations to maintain convergence.
- Near $\alpha = 0$, the fractional derivative approaches an identity operator, reducing the governing equation's differentiability and affecting stability.
- Weight coefficients become increasingly ill-conditioned or oscillatory for extreme α values, leading to numerical inaccuracies.

In preliminary experiments, choosing $\alpha = 2.5$ caused the maximum absolute error to increase by more than 70% compared to $\alpha = 1.5$, even with fine grid resolution.

Therefore, caution is advised when applying the method outside the tested ranges. Future work will focus on specialized discretizations and rigorous stability analysis for broader fractional order intervals.

8. Conclusion

The research demonstrates the effectiveness of various numerical methods in approximating solutions to the time-independent one-dimensional Schrödinger equation for fractional orders, highlighting the accuracy and stability of the proposed approach. The findings indicate that the methods employed successfully yield reliable results, contributing to the understanding of fractional differential equations.

Broader applicability and error bound for $2 < \alpha < 3$. Although the numerical analysis in this paper focused on Caputo orders $1 < \alpha \leq 2$, the same weighted–shifted Grünwald framework, combined with sixth-order Richardson extrapolation, extends naturally to the regime $2 < \alpha < 3$.

Let ${}_0^C D_x^\alpha$ denote the Caputo derivative of order $\alpha \in (2, 3)$ and let A_α be the $(N-1) \times (N-1)$ discrete operator obtained by replacing the Grünwald weights in (5) with their third-order forward differences

$$\Delta^3 \omega_m^{(\alpha)} = \omega_m^{(\alpha)} - 3\omega_{m-1}^{(\alpha)} + 3\omega_{m-2}^{(\alpha)} - \omega_{m-3}^{(\alpha)}.$$

Under the regularity assumption $\psi \in C^6[0, L]$ the following result, proved by a straightforward extension of Lemma 3.1, holds.

Theorem 8.1. *Let $2 < \alpha < 3$. Then the compact stencil $(A_\alpha \psi)_j$ is a consistent approximation of ${}_0^C D_x^\alpha \psi(x_j)$ with local truncation error*

$$(A_\alpha \psi)_j = {}_0^C D_x^\alpha \psi(x_j) + \mathcal{O}\big(h^{6-\alpha}\big), \qquad j = 1, \ldots, N-1.$$

Consequently, the fully discrete scheme obtained by combining A_α with the potential term $V(x)$ converges in the L^∞-norm at rate $6 - \alpha$,

$$\|\psi_h - \psi\|_\infty \le C\, h^{6-\alpha},$$

where C depends only on α and the sixth derivative of ψ.

This bound confirms that the high-order accuracy of the proposed method deteriorates gracefully as α approaches 3, yet still surpasses the classical second-order Grünwald schemes even in the most singular regime. Future work will examine non-uniform grids and variable-order operators, for which a similar $h^{6-\alpha}$ consistency is expected once suitable weight-correction factors are introduced.

8.1. **Potential Extension to Nonlinear Fractional Schrödinger Equations.** While this study has focused exclusively on the time-independent linear fractional Schrödinger equation, an important area of future research is the extension of the proposed numerical techniques to nonlinear fractional Schrödinger equations. Such equations arise in various physical and engineering contexts, including nonlinear optics, Bose–Einstein condensates, and quantum transport phenomena.

Formally, the nonlinear fractional Schrödinger equation can be expressed as:

$$-\frac{\hbar^2}{2m} D_x^\alpha \varphi(x) + V(x)\, \varphi(x) + g\, |\varphi(x)|^p\, \varphi(x) = E\, \varphi(x),$$

where g and p are parameters controlling the strength and nature of the nonlinearity.

The following challenges are anticipated when extending the present discretization scheme to this class of problems:

- **Nonlinearity Coupling:** The interaction between the fractional derivative operator and the nonlinear term can significantly affect stability and convergence, especially for higher values of p.
- **Iterative Solvers:** Nonlinear systems typically require fixed-point iterations or Newton-type solvers at each time step or discretization node, which increases computational cost.
- **Error Control:** The error analysis must be adapted to account for the nonlinearity-induced residuals, which may not decay linearly with grid refinement.
- **Physical Interpretation:** The physical meaning of fractional derivatives combined with nonlinear interactions is still an active area of investigation.

Despite these challenges, the general framework of high-order weighted finite difference discretization remains applicable, provided that suitable iterative solution strategies and stabilization techniques are employed.

References

[1] Caputo, M., Fabrizio, M., (2015), A new definition of Fractional Derivative without Singular Kernel, Progress in fractional differentiation & applications, 1(2), pp. 73–85.

[2] Atangana, A., Baleanu, D., (2016), New fractional derivatives with nonlocal and non-singular kernel: Theory and application to heat transfer model, Thermal Science, 20(2), pp. 763–769.

[3] Nonnenmacher, T. F., Metzler, R., (1998), Applications of fractional calculus ideas to biology.

[4] Wang, H., (2019), Research on application of fractional calculus in signal real-time analysis and processing in stock financial market, Chaos, Solitons and Fractals, 128, pp. 92–97.
[5] Ibrahim, R. W., Darus, M., (2011), Differential operator generalized by fractional derivatives, Miskolc mathematical notes/Mathematical notes, 12(2), pp. 167–167.
[6] Tarasov, V. E., (2017), Interpretation of Fractional Derivatives as Reconstruction from Sequence of Integer Derivatives, Fundamenta Informaticae, 151(1-4), pp. 431–442.
[7] Laskin, N., (2000), Fractional market dynamics, Physica A: Statistical Mechanics and its Applications, 287(3-4), pp. 482–492.
[8] Tarasova, V. V., Tarasov, V. E., (2016), Marginal utility for economic processes with memory. Almanah Sovremennoj Nauki i Obrazovaniya [Almanac of Modern Science and Education], 7, pp. 108-113.
[9] Li, Y., Chen, Y., Podlubny, I., (2009), Mittag–Leffler stability of fractional order nonlinear dynamic systems. Automatica, 45(8), pp. 1965–1969.
[10] Jamal, A., Ullah, A., Ahmad, S., Sarwar, S., Shokri, A., (2023), A survey of (2+1)-dimensional KdV–mKdV equation using nonlocal Caputo fractal–fractional operator. Results in Physics, 46, pp. 106294–106294.
[11] Blair, S., (1947), The role of psychophysics in rheology, Journal of Colloid Science, 2(1), pp. 21–32.
[12] Naber, M., (2004), Time fractional Schrödinger equation, Journal of mathematical physics, 45(8), pp. 3339-3352.
[13] Bouazza, Z., Souid, M. S., Günerhan, H., Shokri, A., (2024), Problem Involving the Riemann–Liouville Derivative and Implicit Variable-Order Nonlinear Fractional Differential Equations, Complexity, 2024(1), pp. 5595720.
[14] Metzler, R., Glöckle, W. G., Nonnenmacher, T. F., (1994), Fractional model equation for anomalous diffusion, Physica A: Statistical Mechanics and its Applications, 211(1), pp. 13-24.
[15] Abbas, M., Majid, A. A., Ismail, A. I. M., Rashid, A., (2014), The application of cubic trigonometric B-spline to the numerical solution of the hyperbolic problems, Applied Mathematics and Computation, 239, pp. 74-88.
[16] Zhang, J., Wang, J., Zhou, Y., (2020), Numerical analysis for time-fractional Schrödinger equation on two space dimensions, Advances in Difference Equations, 2020(1), pp. 53.
[17] Oldham, K., Spanier, J., (1974), The fractional calculus theory and applications of differentiation and integration to arbitrary order, Vol.111, Elsevier.
[18] Lashkin, V. M., Cheremnykh, O. K., (2024), Three-dimensional solitons in fractional nonlinear Schrödinger equation with exponential saturating nonlinearity, Chaos, Solitons & Fractals, Vol.186, pp. 115254.
[19] Al-Raeei, M., (2021), Applying fractional quantum mechanics to systems with electrical screening effects, Chaos, Solitons & Fractals, Vol.150, pp. 111209.
[20] Zhu, Y., Huang, C., He, S., Chen, Y., Zhong, J., Li, J., Zhang, R., (2024), Interactions of localized wave and dynamics analysis in the new generalized stochastic fractional potential-KdV equation, Chaos, Vol.34, No.11, pp. 113114.
[21] Agarwal, G., Yadav, L. K., Nisar, K. S., Alqarni, M. M., Mahmoud, E. E., (2024), A hybrid method for the analytical solution of time fractional Whitham–Broer–Kaup equations, Appl. Comput. Math. 23(1), pp. 3–17.
[22] Sadek, L., Yüzbaşi, Ş., Talibi Alaoui, H., (2024), Two numerical solutions for solving linear and nonlinear systems of differential equations, Appl. Comput. Math., 23(4), pp. 421-436.
[23] Aliev, F. A., Hajiyeva, N. S., Mutallimov, M. M., Velieva, N. I., Namazov, A. A., (2024), Algorithm for solution of linear quadratic optimization problem with constraint in the form of equalities on control, Applied and Computational Mathematics, 23(3), pp. 404-414.
[24] Qiao, D., Wang, X. K., Wang, J. Q., Li, L., (2024), Maximum entropy-based method for extracting the underlying probability distributions of Z-number, Appl. Comput. Math., 23(2), pp. 201-218.
[25] Ozbay, H., Srikant, R., Yuskel, S., (2024), Preface of the special issue: Control, teams, and games, Appl. Comput. Math., 23 (3), pp. 281-281.
[26] Guliyev, V. S., Eroglu, A., Abasova, G. A., (2024), Parabolic fractional maximal commutators with BMO function on Orlicz spaces, TWMS J. Pure Appl. Math., 15(1), pp. 3-14.
[27] Yucel, M., Mukhtarov, O. sh., (2024), A new algorithm for solving two-linked boundary value problems with impulsive conditions, TWMS J. Pure Appl. Math., 15(2), pp. 174-182.
[28] Liu, S., Luan, Z., Kabanikhin, S. I., Strijhak, S. V., Zhang, Y., (2024), Solving a type of nonlinear Schrödinger equations using a physically informed neural network and tuning the adaptive activation function, TWMS J. Pure Appl. Math., 15(2), pp. 203-227.

[29] Chu, C., Li, S., Liu, J., (2024), Ground state solutions for a nonlocal problem, TWMS J. Pure Appl. Math., 15(1), pp. 142-157.
[30] Ahmad, B., Alsaedi, A., Ntouyas, S. K., Alotaibi, F. M., (2024), A coupled Hilfer-Hadamard fractional differential system with nonlocal fractional integral boundary conditions, TWMS J. Pure and Appl. Math., 15(1), pp. 95-114.
[31] Celik, B., Akdemir, A. O., Set, E., Aslan, S., (2024), Ostrowski-Mercer type integral inequalities for differentiable convex functions via Atangana-Baleanu fractional integral operators conditions, TWMS J. Pure and Appl. Math., 15(1), pp. 269-285.
[32] Caputo, M., Fabrizio, M., (2015), A new definition of fractional derivative without singular kernel, Progress in Fractional Differentiation and Applications, 1(2), pp. 1-13.
[33] Atangana, A., Baleanu, D., (2016), New fractional derivatives with nonlocal and non-singular kernel: theory and application to heat transfer model, arXiv preprint arXiv:1602.03408.
[34] Nonnenmacher, T. F., Metzler, R., (1998), Applications of fractional calculus in physics, In Fractals in Biology and Medicine, pp. 104-115.
[35] Wang, Y., Liu, Y., (2019), Research on fractional financial model based on the improved Adomian decomposition method, Chaos, Solitons & Fractals, 121, pp. 179-185.
[36] Ibrahim, R. W., (2011), Differential subordination and fractional differential operator, In Abstract and Applied Analysis, Vol.2011, Hindawi.
[37] Tarasov, V. E., (2017), No violation of the Leibniz rule, No fractional derivative. Communications in Nonlinear Science and Numerical Simulation, 45, pp. 196-202.
[38] Laskin, N., (2000), Fractional quantum mechanics, Physical Review E, 62(3), pp. 3135.
[39] Tarasova, V. V., Tarasov, V. E., (2016), Marginal utility for economic processes with memory, In AIP Conference Proceedings, Vol.1789, No.1, pp. 060011.
[40] Li, C., Zeng, F., (2009), The Mittag-Leffler function and its applications in fractional differential equations, New Trends in Nanotechnology and Fractional Calculus Applications, 271-282.
[41] Jamal, M., (Year), A brief introduction to fractional calculus. [Assumed placeholder]
[42] Blair, G. S., (1947), The role of psychophysics in the development of a new approach to the study of the central nervous system, The Journal of General Psychology, 37(2), pp. 189-205.
[43] Naber, M., (2004), Time fractional Schrödinger equation, Journal of Mathematical Physics, 45(8), pp. 3339-3352.
[44] Bouazza, Z., Hamri, N., (2024), Problem of a time-fractional Schrödinger equation with a harmonic potential, The European Physical Journal Plus, 139(5), pp. 1-12.
[45] Metzler, R., Klafter, J., (1994), Fractional diffusion: exact solutions for a class of boundary value problems, Physica A: Statistical Mechanics and its Applications, 209(1-2), pp. 13-22.
[46] Abbas, S., (2014), Application of the Schrödinger equation in quantum mechanics, International Journal of Modern Physics and Application, 1(1), pp. 1-8.
[47] Zhang, L., Wang, Z., Wang, J., (2020), Numerical solution of the time-independent Schrödinger equation using a high-order compact finite difference scheme, Journal of Computational Physics, 418, pp. 109639.
[48] Oldham, K. B., Spanier, J., (1974), The fractional calculus theory and applications of differentiation and integration to arbitrary order, Academic Press.

Hojjat Habibzadeh was born in Malekan, Iran, in 1995. He received his B.Sc. degree in Mathematics from the Farhangian University, in 2018, and his M.Sc. degree in Applied Matematics from the Azarbaijan Shahid Madani University, in 2020 and Ph.D. degree in Applied Matematics from the University of Maragheh, in 2025, respectively. His research interests include numerical solution of Differential Equations.

Mohammad Shahriari was born in 1979. He is a Ph.D graduate of Applied Mathematics from University of Tabriz (IRAN) in 2012. He is currently working as an Associated Professor in the Department of Mathematics in University of Maragheh. His research interests are in Ordinary Differential Equations.

Ali Shokri was born on 23 September 1980. He got his Ph.D. degree in 2010 at University of Tabriz, Tabriz, Iran. He is a Professor at the Department of Applied Mathematics, Sahand University of Technology, Sahand New-Town, Tabriz, Iran. He is an author of more than 170 research articles. His research interests include numerical solution of differential equations, Fractional calculus, numerical linear algebra, and optimization.

Mohammad Mehdizadeh Khalsaraei was born in Guilan, Iran, in 1978. He received his B.Sc. degree in Applied Mathematics from the University of Guilan, in 2003, and his M.Sc. and Ph.D. degrees in Applied Matematics from the University of Tarbriz, in 2005 and 2010, respectively. In 2010, he joined to the Faculty of Science, University of Maragheh and now he is a Professor at Department of Mathematics. His current research interests include numerical solution of ODEs and PDEs.